

# Discontinuous Galerkin methods for the Laplace-Beltrami operator on point cloud

GUOZHI DONG<sup>1,2</sup>, HAILONG GUO<sup>3</sup>, AND ZUOQIANG SHI<sup>4</sup>

<sup>1</sup>Institute for Mathematics, Humboldt University of Berlin, Unter den Linden 6, 10099 Berlin, Germany

<sup>2</sup> Weierstrass Institute for Applied Analysis and Stochastics, Mohrenstrass 39, 10117 Berlin, Germany

<sup>3</sup>School of Mathematics and Statistics, The University of Melbourne, Parkville, VIC, 3010, Australia

<sup>4</sup>Department of Mathematical Sciences, Tsinghua University, Beijing, 100084, China

## Abstract

A generic geometric error analysis framework for numerical solution of PDEs on submanifolds is established. It requires no global continuity on the patches, and also no embedding of the manifolds and tangential projections. This is different from the existing analysis in the literature, where geometry is assumed to be continuous and errors are mostly residuals of polynomial interpolations. It is applied to analyzing discontinuous Galerkin (DG) methods for the Laplace-Beltrami operator on point clouds. The idea is illustrated through particular examples of an interior penalty DG method for solving the Laplace-Beltrami equation and the corresponding eigenvalue problem with numerical verification.

**AMS subject classifications.** 65D18, 65N12, 65N25, 65N30, 68U05

**Keywords.** Geometric error analysis, discontinuous Galerkin methods, point cloud, Laplace-Beltrami operator, eigenvalue problem

## 1 Introduction

Partial differential equations (PDEs) on manifolds and their numerical methods appear to be a popular topic in recent decades. In particular, starting from [19], surface finite element method (SFEM) has been developed into a rich research direction in numerical analysis, see for instance the survey papers [9, 11, 21] and the references therein. Numerical methods for PDEs on manifolds typically involve two levels of discretization or approximation, first the geometry and its relevant quantities, and second the functions and their derivatives. Research in the literature considers mostly the geometry (manifolds) to be surfaces represented by level set functions (e.g., sign distance functions). The geometry approximations are usually restricted to continuous piecewise polynomial patches which interpolate some underline smooth manifolds. In such a setting, many of the well known numerical methods in planar domains have been generalized to curved spaces or even evolving manifolds. We mention some of the representative works like SFEM, finite volume method, Crouzeix-Raviart element and so on [14, 18, 20, 22, 27]. In particular, we notice some of the recent studies in [4, 12, 13] on discontinuous Galerkin (DG) methods with respect to continuously interpolated piecewise polynomial surfaces. The analysis for the geometric error estimations, developed in the existing works, mostly relies on the fundamental results of [19] for linear SFEM and [14] for higher order ones, which are for interpolation type discretizations. That is, the geometric errors are residuals of local polynomial interpolations. Another restriction in many of the existing works is that the surface gradient and other differential operators is based on the explicit tangential projection from the ambient space onto the tangent spaces of the manifolds to

represent covariant derivatives. That means explicit embedding (e.g., through level set functions) of the manifolds into their ambient Euclidean spaces are assumed to be known. These assumptions limit the application of the existing theory to problems we are going to study in this paper, where manifolds are discretized as point clouds, and numerical methods for solving PDEs on such discrete manifolds need to be developed and analyzed.

This is a practical issue due to the revolutionary development of digital technologies, as point cloud becomes a standard and easy way of sampling surfaces and manifolds in many real-world applications. The existing numerical methods for solving PDEs on point clouds, due to their discrete nature, typically are meshfree type, to name just a few [25, 26]. The method in [26] is based on local polynomial approximation of the surface. The idea is natural and easy to implement, but it is difficult to do theoretical analysis. The point integral method proposed in [25] was proved to be convergent but the convergence rate is low. In this paper, we will develop a (high-order) discontinuous Galerkin (DG) method on point cloud with solid theoretical analysis. However, using DG methods to solve PDEs on point cloud is not directly available. One would need to design algorithms to have a reasonable geometric mesh aligning with the point cloud first. Another difficulty is in theoretical analysis. The geometric assumptions from the existing analysis are typically violated when point cloud representation is used. Thus it calls for new ideas in both algorithm and numerical analysis. This is exactly the goal of this paper, where an algorithmic framework of (discontinuous) Galerkin methods for solving elliptical PDEs on point clouds is proposed, and moreover, a general error analysis tool for such methods is established.

We offer a systematic and generic approach for estimating the geometric errors, which is different from the existing methods in [14, 19]. Our approach considers approximations based on Riemannian metric tensor of the underline manifold, which is independent of the embedding of manifold. The differential operators for functions on the manifold are then represented using local geometric parameterizations and their induced metric tensors. The tangential projection and the embedding information required in many works in the literature, e.g., [14, 19], are not compulsory to know. Moreover, it even does not require the surface patches to be continuous, therefore is capable of dealing with more general geometry and shows more flexibility in geometric approximation and numerical methods. This also serves a starting point for us to study DG methods on point clouds.

In the recent works in [16, 17], the idea of using the Riemannian metric tensor for analyzing geometric errors has been employed in some post-processing schemes for gradient recovery (post-processing of numerical solutions) on manifolds with linear SFEM. In this sense, the geometric error analysis in this paper is a generalization of the works in [16, 17] to higher order SFEMs and DG methods, and to a priori error analysis. We focus on standard but important examples like the Laplace-Beltrami equation and its eigenvalue problem. In our approach, the error analysis to numerical solution of the Laplace-Beltrami equation based on Riemannian metric tensor is more transparent, where the approximation error of the metric tensor sits in the core. Instead of working on an abstract DG method [5, 15, 23, 28], we concentrate on the so-called interior penalty DG method for solving the mentioned two representative problems. We notice that convergence rates of DG methods for eigenvalue problems on planar domain have been studied, e.g., in [3], and higher-order SFEMs for eigenvalue problems were proposed and analyzed in [10]. To the eigenvalue problem, we use also an approach different to both the two works. In order to prove convergence rates of the eigenvalues of the Laplace-Beltrami operator under deformed manifolds, we take into account the invariance of eigenvalues under geometric transformations. Then we follow the classical routine of Babuška-Osborn [7] and apply it to DG methods on discretized manifolds, which concludes with the same theoretical rates as [10] for higher order SFEMs. It was observed in [10] that there is a non-synchronization phenomenon between the geometric error and the function approximation error in terms of eigenvalue convergence rates. Whether the error rates in [10] are sharp or not was an open question. In this paper, we use a simple example (see Remark 4.9) to argue that the theoretical rates we prove for the eigenvalues convergence (therefore also the results in [10]) are actually theoretically optimal.

The rest of the paper is proceeded as follows: Section 2 provides some preliminaries on point clouds and DG methods. Section 3 presents an algorithm for patch reconstruction from point clouds and also the geometric error analysis which generalizes the existing results. Section 4 analyzes the convergence rates of numerical solution of a IPDG method for Laplace-Beltrami equation and its eigenvalue problem on point clouds. Finally the paper is concluded after numerical results and discussions in Section 5. A few technique details are deferred in Appendixes A and B.

## 2 Preliminaries

Let  $\Gamma$  be a smooth (sub-)manifold. To show the main idea, we consider two important exemplary elliptical PDEs on manifolds. The first one is the following Laplace-Beltrami equation: given  $f \in L^2(\Gamma)$ , find  $u \in H^2(\Gamma)$  such that

$$-\Delta_g u + u = f, \quad (2.1)$$

where  $g$  is Riemannian metric of  $\Gamma$ . The weak version of problem (2.1) is to find  $u \in H^1(\Gamma)$  solving the following equation

$$\mathcal{A}(u, v) = (f, v), \quad \text{for all } v \in H^1(\Gamma). \quad (2.2)$$

where

$$\mathcal{A}(w, v) = \int_{\Gamma} (\nabla_g w \cdot \nabla_g v + uv) dA_g, \quad (f, v) = \int_{\Gamma} f v dA_g.$$

In the second study, we consider the eigenvalue problem associated to the Laplace-Beltrami operator on  $\Gamma$ : find pairs  $(\lambda, u) \in (\mathbb{R}^+, H^2(\Gamma))$  such that

$$-\Delta_g u = \lambda u. \quad (2.3)$$

The eigenvalues are assumed to be ordered so that  $0 = \lambda_1 \leq \lambda_2 \leq \dots \leq \lambda_n \leq \dots$ , and the corresponding eigenfunctions are normalized to satisfy  $\|u_i\|_{L^2(\Gamma)} = 1$ . The weak formulation of (2.3) read as: find  $(\lambda, u) \in (\mathbb{R}^+, H^1(\Gamma))$  with  $\|u\|_{L^2(\Gamma)} = 1$  such that

$$\int_{\Gamma} \nabla_g u \cdot \nabla_g v dA_g = \lambda \int_{\Gamma} u v dA_g \quad \text{for all } v \in H^1(\Gamma). \quad (2.4)$$

Well-posedness of the above problems have been discussed for instance in [6]. Our goal here is to develop numerical methods for such type of PDEs when the information of  $\Gamma$  is given in the form of point cloud sampling.

### 2.1 Basics of point clouds and manifolds

Let  $\Sigma = \{\xi_1, \xi_2, \dots, \xi_N\}$  be set of points which is sampled from a closed smooth manifold  $\Gamma$ . To make concrete discussions, we consider  $\Gamma \subset U \subset \mathbb{R}^3$ . We also assume there is a closed polygon consisting of planar domains (e.g., triangles)  $\{\Omega_h^j\}$ . We denote  $\Omega_h = \bigcup_j \Omega_h^j$ . We will abuse a bit of notations in the paper, as  $\Omega_h^j$  denotes *both a planar triangle and also the corresponding hyperplane generated from the triangle*. Then there exist some bijective smooth mapping  $\pi : \Omega_h \rightarrow \Gamma$ . This mapping  $\pi$  induces a metric tensor  $g$  on  $\Gamma$  through the following relation:

$$g \circ \pi = (\nabla \pi)^\top \nabla \pi. \quad (2.5)$$

Note that  $\pi$  is not necessarily a global mapping, which may be defined in a locally patchwise fashion. It turns out that this relation is important for the error analysis in this paper.

We also notice that mappings from  $\Omega_h$  to  $\Gamma$  are not unique. In fact, there are infinitely many different choices, which are called isomorphisms. However, we focus on this particular mapping  $\pi : U \rightarrow \Gamma$  in (2.6), of which the pre-image domain is restricted to  $\Omega_h$ :

$$\pi(x) = x - d(x)\nu(x), \quad (2.6)$$

where  $\nu(x) = \nu(\pi(x))$  is the unit outward normal vector at the point  $\pi(x)$  on  $\Gamma$ , and  $d(x)$  is the sign distance function of  $\Gamma$ . Particularly, we assume  $\Omega_h$  to be close enough to  $\Gamma$ , such that the projection  $\pi$  is bijective between  $\Omega_h^j$  and  $\Gamma_h^j \subset \Gamma$ . We use  $\Gamma_h := \bigcup_j \Gamma_h^j$  to denote the set of curved triangles on  $\Gamma$ . The Jacobian can be computed by  $\nabla \pi(x) = P_\tau - d(x)H$ , where  $H$  is the second fundamental form, whose eigenvalues are the principal curvatures  $\kappa$  of  $\Gamma$ .  $P_\tau$  is the tangential projection and it satisfies  $P_\tau \nabla \pi(x) = \nabla \pi(x) = \nabla \pi(x)P_\tau$ .

If  $\pi : \Omega_h \rightarrow \Gamma_h$  is bijective, then  $\nabla \pi(x)$  is invertible. This is true provided that  $d\kappa < 1$ . That means the distance of  $\Omega_h$  to  $\Gamma_h$  is inversely proportional to the curvature at the projected point. In

particular, singular points (where  $\kappa$  are unbounded) of the manifold should be coincide with their projection points on  $\Omega_h$ . In order to develop discontinuous Galerkin methods, we shall consider piecewise polynomial patches of order  $k$  approximating given point clouds. Therefore, we use local polynomial functions reconstructed from each local group of points  $\{\xi_i\}_i \subset \Sigma$ , and denote such polynomial surface patches by  $\hat{\Gamma}_h^{k,j}$ . In Algorithm 1, we provide such a reconstruction from the given point cloud representation of  $\Gamma$  to have  $\pi_h^k : \Omega_h \rightarrow \hat{\Gamma}_h^k$ . Using the parametrization map  $\pi$ , the gradient of scalar function on manifolds can be calculated as

$$(\nabla_g v) \circ \pi = \nabla \pi(g^{-1} \circ \pi) \nabla \bar{v}. \quad (2.7)$$

Here  $\bar{v} = v \circ \pi$ , and  $\nabla$  is the gradient operator on the planar parametric domain  $\Omega$ , when it applies to vector valued functions, then it is the Jacobian. Note that this is a different expression of surface gradient as in many references of surface finite element methods like [14, 19]. It allows us to develop a brand new numerical analysis framework for investigating PDEs on surfaces.

## 2.2 DG methods on point cloud

Discontinuous Galerkin methods for elliptical PDEs can be traced back to several seminal works, e.g., [5, 15, 23, 28]. In this paper, we shall focus on an interior penalty discontinuous Galerkin method (IPDG) and generalize it for numerical solutions of PDEs on point cloud.

The standard formulations of DG methods in a surface setting have been studied in [4, 13], a bilinear form of which is recalled as follows:

$$\begin{aligned} \mathcal{A}_h^{k,l}(u_h, v_h) := & \sum_j \int_{\hat{\Gamma}_h^{k,j}} \left( \nabla_{g_h^k} u_h \cdot \nabla_{g_h^k} v_h + u_h v_h \right) dA_{g_h^k} \\ & - \sum_{e_h^k \in \hat{\mathcal{E}}_h} \int_{\tilde{e}_h^k} \left( \{(\nabla_{g_h^k} u_h \cdot n_h)\}[v_h] + \{(\nabla_{g_h^k} v_h \cdot n_h)\}[u_h] - \frac{\beta}{h} [u_h][v_h] \right) dE_{g_h^k}. \end{aligned} \quad (2.8)$$

Here  $\hat{\mathcal{E}}_h$  denotes the edge set contains all the edges from the curved triangles in  $\hat{\Gamma}_h^k$ , and  $\beta$  denotes the stabilization parameter. For quantity  $q$  defined on  $(\tilde{e}_h^{k,j})^\pm \in \partial\Gamma_h$ , the averaging is defined to be  $\{q\} := \frac{1}{2}(q^+ + q^-)$  and the jump is defined to be  $[q] := q^+ - q^-$ . Note that the bilinear form (2.8) has been considered already in [4] though different notations are used there. The main difference is that in [4], the exact manifolds are assumed to be known and  $\hat{\Gamma}_h^k$  is assumed to be piecewise polynomial interpolation of  $\Gamma_h$ . However, different situations are confronted in general for point clouds. First of all,  $\Gamma$  is not known, and thus  $\hat{\Gamma}_h^k$  is not immediately available for a given point clouds. We need to construct such an approximation from a set of scattered points in order to apply a Galerkin type numerical method. This shall be discussed in Section 3.1. Secondly, it might be the case that the reconstructed patches are separated and they might share no common edges with their neighbors. This is usually the case resulting from the local geometric reconstruction of the manifolds through point cloud. Therefore the DG methods in the literature can not be applied directly. In this regard, we need to write down a more general computational formula. To do so, we pull back all the calculations onto the parametric domain  $\Omega_h$ . Then we have the following DG form for general problems on manifolds:

$$\begin{aligned} \mathcal{A}_h^{k,l}(u_h, v_h) := & \sum_j \int_{\Omega_h^j} ((\nabla \bar{u}_h)^\top (g_h^k)^{-1} \nabla \bar{v}_h + \bar{u}_h \bar{v}_h) \sqrt{|g_h^k|} dA + \frac{\beta}{h} \sum_{e_h \in \mathcal{E}_h} \int_{e_h} [\bar{u}_h][\bar{v}_h]\{l_{g_h^k}\} dE \\ & - \sum_{e_h \in \mathcal{E}_h} \int_{e_h} \{(\nabla \bar{u}_h)^\top (g_h^k)^{-1} (\partial \pi_h^k)^\top n_h\}[\bar{v}_h l_{g_h^k}] + \{(\nabla \bar{v}_h)^\top (g_h^k)^{-1} (\partial \pi_h^k)^\top n_h\}[\bar{u}_h l_{g_h^k}] dE. \end{aligned} \quad (2.9)$$

Note that in the parametric domain,  $e_h^j$  between two neighbored triangles are unique, which is similar to the standard DG methods. However, different metrics apply to the common edge. This has been reflected in the bilinear form (2.9) where  $l_{g_h^k}^+$  and  $l_{g_h^k}^-$  might be different.

In order to have a comparison with the DG bilinear form on the exact manifolds  $\Gamma$ , we also use

the following parametric presentation

$$\begin{aligned}\mathcal{A}_h^l(u_h, v_h) := & \sum_j \int_{\Omega_h^j} ((\nabla \bar{u}_h)^\top g^{-1} \nabla \bar{v}_h + \bar{u}_h \bar{v}_h) \sqrt{|g|} dA + \frac{\beta}{h} \sum_{\bar{e}_h \in \bar{\mathcal{E}}_h} \int_{\bar{e}_h} [\bar{u}_h][\bar{v}_h] l_g dE \\ & - \sum_{\bar{e}_h \in \bar{\mathcal{E}}_h} \int_{\bar{e}_h} ((\nabla \bar{u}_h)^\top g^{-1} (\partial \pi)^\top n)[\bar{v}_h] + ((\nabla \bar{v}_h)^\top g^{-1} (\partial \pi)^\top n)[\bar{u}_h]) l_g dE.\end{aligned}\quad (2.10)$$

In the following, we denote  $\beta_h := \frac{\beta}{h}$ . Note that the difference between (2.10) and (2.9) is that the edge metric scaling  $l_g$  is the same on every shared edge while  $l_{g_h^k}$  in general might be not coincide. In that case the formula in (2.10) is just a rewriting of the formula in (2.8) by replacing the metric tensor  $g$  with  $g_h^k$ .

### 3 Geometry reconstruction and its error analysis

In the above discussion, we have assumed that there exists surface patches for defining our discontinuous Galerkin methods. Different from the standard numerical methods on surfaces or manifolds, this local patch is not trivially given beforehand. Therefore, in the following, we provide first an algorithm for generating piecewise local polynomial patches to approximate the unknown manifold from the point cloud.

#### 3.1 Patch reconstruction from point cloud

We first need to find an initial polygon  $\Omega_h \subset U$  which close enough to  $\Gamma$ . For this, we use tools from computational geometry, e.g., CGAL [2]. Choose a fixed discretization size  $h$ . Suppose  $\Omega_h = \bigcup_j \Omega_h^j$  be some polygon close enough to  $\Gamma$ , so that  $\pi : \Omega_h \rightarrow \Gamma_h$  defined in (2.6) is bijective. The algorithm for constructing element patches is given in Algorithm 1.

Note that  $\Gamma_h^{k,j}$  consists of piecewise polynomial patches, but not interpolating  $\Gamma_h$ . Step 2 is only for computational convenience afterwards in the (discontinuous) Galerkin methods, which is not required for the analysis. In Algorithm 1,  $\psi_h^j$  is still yet to compute. For a given point  $x \in \Omega_h^j$  over the parametric domain, we compute the point  $\psi \in \Gamma_h^{k,j}$  such that  $\psi(x) - x = -d_h^k(x)\nu_h^{k,j}(x)$ , where  $\nu_h^{k,j}$  denotes the unit outward normal vector of the local polynomial graph, and  $d_h^k$  is the length of the vector  $\psi - x$ . Since  $\psi = (\psi_1, \psi_2, \psi_3)$  is a local polynomial graph, i.e.,  $\psi_3 = p_h^{k,j}(\psi_1, \psi_2)$ , then using this local coordinates,  $x = (x_1, x_2, 0)$ . Also notice that  $d(x) = \sqrt{(\psi_1 - x_1)^2 + (\psi_2 - x_2)^2 + (\psi_3)^2}$ , and  $\nu(x) = \frac{(-\partial_1 p_h^{k,j}, -\partial_2 p_h^{k,j}, 1)^\top}{\sqrt{(\partial_1 p_h^{k,j})^2 + (\partial_2 p_h^{k,j})^2 + 1}}$ . This leads us to the following nonlinear system

$$\begin{aligned}\psi_3 \partial_1 p_h^{k,j}(\psi_1, \psi_2) + \psi_1 - x_1 &= 0 \\ \psi_3 \partial_2 p_h^{k,j}(\psi_1, \psi_2) + \psi_2 - x_2 &= 0 \\ \psi_3 - p_h^{k,j}(\psi_1, \psi_2) &= 0.\end{aligned}\quad (3.2)$$

We rewrite the above system in a compact way as  $M(\psi) = 0$  which can be then solved using Newton's method. For Newton's method, we reduce the above system to a two variables equation

$$\begin{aligned}M_1(\psi_1, \psi_2) &= p_h^{k,j}(\psi_1, \psi_2) \partial_1 p_h^{k,j}(\psi_1, \psi_2) + \psi_1 - x_1 = 0 \\ M_2(\psi_1, \psi_2) &= p_h^{k,j}(\psi_1, \psi_2) \partial_2 p_h^{k,j}(\psi_1, \psi_2) + \psi_2 - x_2 = 0\end{aligned}\quad (3.3)$$

which then gives rise to the following iterations for some initial guess, e.g.,  $(\psi_1^0, \psi_2^0)^\top = (x_1, x_2)^\top$ :

$$(\psi_1^{m+1}, \psi_2^{m+1})^\top = (\psi_1^m, \psi_2^m)^\top - (\nabla M^m)^{-1} (M_1^m, M_2^m)^\top; \quad \psi_3^{m+1} = p_h^{k,j}(\psi_1^{m+1}, \psi_2^{m+1}). \quad (3.4)$$

where  $M_i^m = M_i(\psi_1^m, \psi_2^m)$ , and  $\nabla M^m = \begin{pmatrix} \partial_1 M_1(\psi_1^m, \psi_2^m) & \partial_1 M_2(\psi_1^m, \psi_2^m) \\ \partial_2 M_1(\psi_1^m, \psi_2^m) & \partial_2 M_2(\psi_1^m, \psi_2^m) \end{pmatrix}$  which is a symmetric matrix. Note that its inverse matrix can be explicitly calculated

$$(\nabla M^m)^{-1} = \frac{1}{\det(\nabla M^m)} \begin{pmatrix} \partial_2 M_2(\psi_1^m, \psi_2^m) & -\partial_1 M_2(\psi_1^m, \psi_2^m) \\ -\partial_2 M_1(\psi_1^m, \psi_2^m) & \partial_1 M_1(\psi_1^m, \psi_2^m) \end{pmatrix}.$$

The Newton iterations are terminated once an expected accuracy level is reached (in our examples, we choose it to be  $10^{-14}$ ).

---

**Algorithm 1** Patch reconstruction from point cloud

---

Step 1. Let  $J$  is the total number of small triangles of  $\Omega_h$ . For  $j \in J$ , do

1. For each  $\Omega_h^j$ , pick its barycenter  $c^j$ , and select a set of  $m$  points in  $\Sigma$  which are close to  $\Omega_h^j$  and uniformly distributed, denoted by  $\xi_1^j, \xi_2^j, \dots, \xi_m^j$ . Thus  $(\xi_i^j)_{i=1, \dots, m}$  is  $\mathcal{O}(h^2)$  close to  $\Omega_h^j$ .
2. Let  $c^j$  be the origin, and choose a local coordinate system where the hyperplane of  $\Omega_h^j$  is the transverse plane. Then we change the coordinates of  $\{\xi_i^j\}_{i=1}^m$  according to the new local system. In the local coordinates,  $\{\xi_i^j\}_{i=1}^m$  is represented as  $(s_i^j, v_i^j)$  for  $s_i^j \in \Omega_h^j$ .
3. Then approximate (interpolate) the points using an  $k^{th}$  order polynomial function graph defined on the hyperplane of  $\Omega_h^j$ . That is to find  $p_h^{k,j}$  such that

$$p_h^{k,j} = \operatorname{argmin}_p \frac{1}{m} \sum_{i=1}^m |p(s_i^j) - v_i^j|^2 \text{ over } p \in \mathbb{P}^k(\Omega_h^j). \quad (3.1)$$

We choose the number  $m$  in the first step is sufficiently large, so that  $p_h^{k,j}$  is uniquely determined.

4. Select some interpolating points  $(x_k^j)_k \subset \Omega_h^j$  in the parameter domain. Typically, those points  $x_k^j$  are chosen according to the polynomial degree.
5. Compute  $\psi_k^j = \pi_h^k(x_k^j)$  for those selected points  $x_k^j \in \Omega_h^j$  using the iterations described in (3.4) to get the corresponding points  $\psi_k^j$ .

Step 2. Apply a simple averaging of reconstructed nodal points on every common edge of  $\Omega_h^{j_1}$  and  $\Omega_h^{j_2}$  for all possible  $j_1$  and  $j_2$ .

Step 3. The generated nodal points are used to have the piecewise polynomial patches over every  $\Omega_h^j$  to approximate  $\Gamma_h^j$  using polynomial interpolation. This piecewise polynomial patch is then denoted as  $\hat{\Gamma}_h^{k,j}$ .

---

### 3.2 Geometric error analysis

One difficulty in numerical analysis for problems on manifolds is that there are error sources in the discretization of both geometry and function spaces defined on the geometry. In the literature, most of the cases, the geometric error are assumed to be interpolation residuals. However, in the case of point clouds, this is usually not the case. In order to apply (discontinuous) Galerkin methods, we first reconstruct a set of patches from the point cloud which approximate the original manifold  $\Gamma$ . To proceed with the error analysis, we consider the following assumptions.

**Assumption 3.1.** *Let  $h$  be the largest diameter of the triangles on  $\Omega_h$ . We consider the following assumptions on the geometry.*

- (1). *The points in the point cloud are distributed uniformly on  $\Gamma$ .  $\Gamma$  is  $C^{k_0}$  smooth, for  $k_0 \geq \max\{k, 2\}$ , where  $k$  is the polynomial order of the surface reconstruction, and it has uniformly bounded curvature.*
- (2). *The polygon  $\Omega_h$  is  $\mathcal{O}(h^2)$  close to the manifold  $\Gamma_h$ . This is understood in the sense that for every selected pair  $\Omega_h^j$  and  $\Gamma_h^j$ , we have  $|\pi(x) - x| \leq Ch^2$  with some uniform constant  $C$  independent of  $h$  and  $x$ . Thus the points in the point cloud are also  $\mathcal{O}(h^2)$  close to  $\Omega_h$  in that sense.*
- (3). *There exist curved triangles  $\Gamma_h^j \subset \Gamma$  of diameter  $h$  connecting neighbored points along the manifold. These triangles are shape regular, in particular,  $\Gamma = \Gamma_h = \cup_{j \in J} \Gamma_h^j$ .*

We now show some of the approximation property for the nodal points  $(\psi^i)_{i \in \mathbb{N}}$  reconstructed from Step 1 in Algorithm 1. In view of the equation in (3.2), the partial differential operators seem to reducing the approximation accuracy of the polynomial functions  $p_h^j$  after the Newton projection. In the following, we show that surprisingly this is *not* the case as long as the Newton iterations in (3.4) converge sufficiently.

Before we prove the proposition, we provide an auxiliary lemma on polynomial approximation of scattering points. This is a standard result which is available in many references, e.g., [29]. For completeness, a proof is provided in Appendix A.

**Lemma 3.2.** *Let the local patches be reconstructed as in Algorithm 1, which are function graphs of  $k^{\text{th}}$  order polynomials, and let Assumption 3.1 hold for the point cloud. If the selected points are uniformly distributed for every reconstructed patch. Then, the fitting polynomial function satisfies*

$$\|p_h^{k,j} - p^j\|_{L^\infty(\Omega_h^j)} \leq Ch^{k+1} \quad \text{and} \quad \|\nabla p_h^{k,j} - \nabla p^j\|_{L^\infty(\Omega_h^j)} \leq Ch^k \quad \text{for all } j \in J. \quad (3.5)$$

where  $p_h^{k,j}$  and  $p^j$  are the local polynomial function and the precise function whose graph gives the exact patch on  $\Gamma$ , respectively.

Here and also in the following sections, we always use  $C$  to denote some  $h$  independent generic constant, which may take different values in different estimates. Now, we are in the position to present a fundamental approximation result.

**Proposition 3.3.** *Let Assumption 3.1 hold. Suppose the Newton iteration in Algorithm 1 converge sufficiently. Then the reconstructed nodal points  $(\psi^i)_{i \in \mathbb{N}}$  satisfy the following approximation property to the precise nodal points  $(\xi^i)_{i \in \mathbb{N}} \subset \Gamma$*

$$|\psi^i - \xi^i| \leq Ch^{k+1}. \quad (3.6)$$

In particular

$$|\psi_\Omega^i - \xi_\Omega^i| \leq Ch^{k+2}, \quad (3.7)$$

where  $\psi_\Omega^i$  and  $\xi_\Omega^i$  are the components projected onto the parametric domain  $\Omega_h$ .

*Proof.* Recall the formula (3.2). Then we have

$$\psi_\Omega^i - \xi_\Omega^i = p(\xi_\Omega^i) \nabla p(\xi_\Omega^i) - p_h^k(\psi_\Omega^i) \nabla p_h^k(\psi_\Omega^i) \quad \text{and} \quad \psi_1^i - \xi_1^i = p_h^k(\psi_\Omega^i) - p(\xi_\Omega^i) \quad (3.8)$$

where  $p_h^k : \Omega_h \rightarrow \mathbb{R}$  is the reconstructed local polynomial patch in Algorithm 1, and  $p : \Omega_h \rightarrow \mathbb{R}$  is the counterpart of  $p_h^k$  associated to the patch on  $\Gamma$ . Note that  $p$  and  $p_h^k$  satisfy the estimate

from Lemma 3.2. In particular, they satisfy  $\|p\|_{L^\infty(\Omega_h)} \leq Ch^2$  and  $\|p_h^k\|_{L^\infty(\Omega_h)} \leq Ch^2$ . In the following we always consider the  $L^\infty(\Omega_h)$  norm, which should be uniform on the index  $j$  and thus the subscript on  $j$  is ignored here and next. Based on the triangle inequality, (3.8) indicates

$$\begin{aligned} \|\psi_\Omega^i - \xi_\Omega^i\| &\leq \|\nabla p(\xi_\Omega^i)\| \|p(\xi_\Omega^i) - p_h^k(\xi_\Omega^i)\| + L \|\nabla p(\xi_\Omega^i)\| \|\psi_\Omega^i - \xi_\Omega^i\| \\ &\quad + \|p_h^k(\psi_\Omega^i)\| \|\nabla p(\xi_\Omega^i) - \nabla p_h^k(\xi_\Omega^i)\| + L' \|p_h^k(\psi_\Omega^i)\| \|\psi_\Omega^i - \xi_\Omega^i\| \end{aligned}$$

where  $L$  and  $L'$  are the local Lipschitz constants of the functions  $p$  and  $\nabla p_h^k$  over  $\Omega_h$ , respectively, which are of the magnitude  $h$  and 1, respectively, thus uniformly bounded. Rearranging the above inequality, we have

$$\begin{aligned} &(1 - L \|\nabla p(\xi_\Omega^i)\| - L' \|p_h^k(\psi_\Omega^i)\|) \|\psi_\Omega^i - \xi_\Omega^i\| \\ &\leq \|\nabla p(\xi_\Omega^i)\| \|p(\xi_\Omega^i) - p_h^k(\xi_\Omega^i)\| + \|p_h^k(\psi_\Omega^i)\| \|\nabla p(\xi_\Omega^i) - \nabla p_h^k(\xi_\Omega^i)\| \end{aligned}$$

The above inequality tells that for sufficiently small  $h_0$ , there exists a constant  $C$  such that

$$C \leq (1 - L \|\nabla p(\xi_\Omega^i)\| - L' \|p_h^k(\psi_\Omega^i)\|) \quad \text{for all } h \leq h_0.$$

Then we have

$$\|\psi_\Omega^i - \xi_\Omega^i\| \leq \frac{1}{C} (\|\nabla p(\xi_\Omega^i)\| \|p(\xi_\Omega^i) - p_h^k(\xi_\Omega^i)\| + \|p_h^k(\psi_\Omega^i)\| \|\nabla p(\xi_\Omega^i) - \nabla p_h^k(\xi_\Omega^i)\|)$$

which confirms (3.7), i.e.,  $\|\psi_\Omega^i - \xi_\Omega^i\| \leq Ch^{k+2}$ . Back to the second part of (3.8), similarly we have

$$\|\psi_1^i - \xi_1^i\| \leq \|p_h^k(\psi_\Omega^i) - p(\psi_\Omega^i)\| + \|p(\psi_\Omega^i) - p(\xi_\Omega^i)\| \leq Ch^{k+1} + L \|\psi_\Omega^i - \xi_\Omega^i\|.$$

This concludes the statement in (3.6) by noticing that

$$\|\psi^i - \xi^i\| \leq \|\psi_1^i - \xi_1^i\| + \|\psi_\Omega^i - \xi_\Omega^i\|.$$

□

With the error bounds (3.6) and (3.7), we are able to estimate further the geometric approximation errors.

**Lemma 3.4.** *Let the same assumptions as Proposition 3.3 hold. Let  $\pi : \Omega_h \rightarrow \Gamma_h$  and  $\pi_h^k : \Omega_h \rightarrow \hat{\Gamma}_h^k$  be the mapping associated to the original patches on  $\Gamma$  and the reconstructed polynomial patches, respectively. The reconstruction is done by interpolating the reconstructed nodal points from Algorithm 1. Then we have the following error bounds:*

$$\begin{aligned} \|\nabla \pi - \nabla \pi_h^k\|_{L^\infty(\Omega_h)} &\leq Ch^k, \quad \|(\nabla \pi - \nabla \pi_h^k)_\Omega\|_{L^\infty(\Omega_h)} \leq Ch^{k+1}, \\ \|(\nabla \pi)_1\|_{L^\infty(\Omega_h)} &\leq Ch \quad \text{and} \quad \|(\nabla \pi_h^k)_1\|_{L^\infty(\Omega_h)} \leq Ch. \end{aligned} \quad (3.9)$$

Here  $\nabla \pi$ , the Jacobian, is considered to be a  $3 \times 2$  matrix, and  $(\nabla \pi)_1$  is the first row of  $\nabla \pi$ , a  $1 \times 2$  vector, and  $(\nabla \pi)_\Omega$  is the second and third rows of  $\nabla \pi$ , thus a  $2 \times 2$  matrix, corresponding to the components in the parameter domain.

*Proof.* Based on Lemma 3.2, and let  $\tilde{\pi}_h^k$  be the polynomial patch by interpolating the exact nodal points  $\{\xi^i\}$ . Therefore we have that  $\tilde{\pi}_h^k = \sum_{i=1}^m \xi^i \phi_i$  and  $\pi_h^k = \sum_{i=1}^m \psi^i \phi_i$  where  $m$  is the number of nodal points depending on the interpolating polynomial orders, and  $(\phi_i)_i$  are the Lagrange polynomial bases. Then we have

$$\|\nabla \tilde{\pi}_h^k - \nabla \pi_h^k\|_{L^\infty(\Omega_h)} \leq Ch^k.$$

To see the first estimate in (3.9), we simply use the triangle inequality

$$\|\nabla \pi - \nabla \pi_h^k\|_{L^\infty(\Omega_h)} \leq \|\nabla \pi - \nabla \tilde{\pi}_h^k\|_{L^\infty(\Omega_h)} + \|\nabla \tilde{\pi}_h^k - \nabla \pi_h^k\|_{L^\infty(\Omega_h)} \leq C_1 h^k.$$

For the second estimate we consider  $(\nabla \tilde{\pi}_h^k - \nabla \pi_h^k)_\Omega = \sum_{i=1}^m (\psi_\Omega^i - \xi_\Omega^i) \phi_i$ . The estimate follows immediately again from the triangle inequality

$$\|(\nabla \pi - \nabla \pi_h^k)_\Omega\|_{L^\infty(\Omega_h)} \leq \|(\nabla \pi - \nabla \tilde{\pi}_h^k)_\Omega\|_{L^\infty(\Omega_h)} + \|(\nabla \tilde{\pi}_h^k - \nabla \pi_h^k)_\Omega\|_{L^\infty(\Omega_h)}.$$

The third and the forth estimates follows from the fact that  $\psi_1^i$  and  $\xi_1^i$  are both of order  $\mathcal{O}(h^2)$  over the domain  $\Omega_h$ . □

To simplify notations, we will not distinguish metric tensors  $g$  and  $g_h^k$  with  $g \circ \pi$  and  $g_h^k \circ \pi_h^k$  in the following. In the next proposition, we shall reveal that the metric tensor resulted from the reconstructed polynomial patch enjoys one order higher accuracy in the approximation comparing to the Jacobian.

**Proposition 3.5.** *Given the same condition as Lemma 3.4, we have*

$$\begin{aligned} \|g^{-1}(g - g_h^k)\|_{L^\infty} &\leq Ch^{k+1}, \quad \left\| \frac{\sqrt{|g|} - \sqrt{|g_h^k|}}{\sqrt{|g|}} \right\|_{L^\infty} \leq Ch^{k+1}, \\ \left\| \frac{l_{g_h^k} - l_g}{l_g} \right\|_{L^\infty} &\leq Ch^{k+1} \quad \text{and} \quad \|g^{-1}(\nabla\pi)^\top n - (g_h^k)^{-1}(\nabla\pi_h^k)^\top n_h^k\|_{L^\infty} \leq Ch^{k+1}, \end{aligned} \quad (3.10)$$

where  $n$  and  $n_h^k$  are the unit normal vectors on the edges of the curved triangles, which are tangential to the surfaces  $\Gamma$  and  $\hat{\Gamma}_h^k$ , respectively.

*Proof.* Recall that  $g \circ \pi = (\partial\pi)^\top \partial\pi$ , and  $g_h^k \circ \pi_h^k = (\partial\pi_h^k)^\top \partial\pi_h^k$ . Then

$$\begin{aligned} g^{-1}(g - g_h^k) &= g^{-1}((\partial\pi)^\top \partial\pi - (\partial\pi_h^k)^\top \partial\pi_h^k) \\ &= g^{-1} \frac{1}{2} (((\partial\pi)^\top + (\partial\pi_h^k)^\top)(\partial\pi - \partial\pi_h^k) + ((\partial\pi)^\top - (\partial\pi_h^k)^\top)(\partial\pi + \partial\pi_h^k)) \\ &= g^{-1} \frac{1}{2} (((\partial\pi)^\top + (\partial\pi_h^k)^\top)_\Omega (\partial\pi - \partial\pi_h^k)_\Omega + ((\partial\pi)^\top - (\partial\pi_h^k)^\top)_\Omega (\partial\pi + \partial\pi_h^k)_\Omega) \\ &\quad + g^{-1} \frac{1}{2} (((\partial\pi)^\top + (\partial\pi_h^k)^\top)_1 (\partial\pi - \partial\pi_h^k)_1 + ((\partial\pi)^\top - (\partial\pi_h^k)^\top)_1 (\partial\pi + \partial\pi_h^k)_1) \end{aligned}$$

Note that due to the assumptions on  $\Gamma$ ,  $g^{-1}$  is uniformly bounded independent of  $h$ . Then using the estimate from Lemma 3.4, we have the following

$$\|(\partial\pi - \partial\pi_h^k)_\Omega\|_{L^\infty(\Omega_h)} \leq Ch^{k+1} \quad \text{and} \quad \|((\partial\pi)^\top - (\partial\pi_h^k)^\top)_1\|_{L^\infty(\Omega_h)} \leq Ch^k$$

and  $\|(\partial\pi + \partial\pi_h^k)_\Omega\|_{L^\infty(\Omega_h)} \leq C$  is uniformly bounded for some constant  $C$  independent of  $h$  and

$$\|((\partial\pi)^\top + (\partial\pi_h^k)^\top)_1\|_{L^\infty(\Omega_h)} \leq Ch.$$

These together give us the first estimate. The second and the third estimates are consequences derived immediately from the first estimate. We skip the details here. For the forth one, notice that  $n = \nabla\pi e_n$  and  $n_h^k = \nabla\pi_h^k e_{n_h}$  where  $e_n$  and  $e_{n_h}$  both are  $2 \times 1$  vectors defined on the edges of the triangles in the common planar parameter domain  $\Omega_h$ . Since both  $\Gamma_h$  and  $\hat{\Gamma}_h^k$  have uniformly bounded curvature, then the lengths of  $e_n$  and  $e_{n_h}$  are uniformly bounded from above and also bounded away from zero. Thus

$$g^{-1}(\nabla\pi)^\top n - (g_h^k)^{-1}(\nabla\pi_h^k)^\top n_h^k = g^{-1}g e_n - (g_h^k)^{-1}g_h^k e_{n_h} = e_n - e_{n_h}.$$

On the other hand, due to the fact that  $n$  and  $n_h$  are unitary vectors, and  $g$  is positive definite, we have

$$e_n^\top g e_n = e_{n_h}^\top g_h^k e_{n_h} = 1 \quad \Rightarrow \quad (e_n - e_{n_h})^\top g (e_n + e_{n_h}) = e_{n_h}^\top (g_h^k - g) e_{n_h}$$

Due to the positive definiteness of the metric tensor  $g$ , the above relation indicates that

$$\|e_n - e_{n_h}\|_{L^\infty(\Omega_h)} \leq C \|g - g_h^k\|_{L^\infty(\Omega_h)}$$

which then gives us the estimate that

$$\|g^{-1}(\nabla\pi)^\top n - (g_h^k)^{-1}(\nabla\pi_h^k)^\top n_h^k\|_{L^\infty(\Omega_h)} = \|e_n - e_{n_h}\|_{L^\infty(\Omega_h)} = \mathcal{O}(h^{k+1}).$$

□

**Remark 3.6.** We note that surprisingly the two error estimates of the Jacobian  $\|\partial\pi - \partial\pi_h^k\|_{L^\infty(\Omega_h)}$  and the metric tensors  $\|g - g_h^k\|_{L^\infty(\Omega_h)}$  are not of the same order, even though the metric tensors are represented by product of Jacobian and its transpose through (2.5). This is due to the assumption that the local patches parameterized by  $\Omega_h$  are in the  $\mathcal{O}(h^2)$  neighborhood of  $\Omega_h$ , which then results the estimate in (3.7). For the interpolating polynomial patches of a smooth manifold, the estimates in (3.6) and (3.7) are naturally fulfilled, while for arbitrary approximations, this is not granted. Therefore, with only the condition (3.6), it is in general not sufficient to prove the results in Proposition 3.5. An immediate example one may think is a right-angled triangle with two orthogonal edges of length  $h$ , while another right-angled triangle in the same plane with two orthogonal edges of length  $h + h^2$ . Then the ratio of the areas of the two triangles is  $1 + 2h + h^2$  which does not give the results in Proposition 3.5. This also explains why the closeness property in (3.7) which we prove for Algorithm 1 is important.

## 4 Error estimates of DG methods

### 4.1 Function spaces associated to DG methods

In order to conduct error analysis for the DG method formulated in (2.9), we introduce necessary function spaces and also their associated norms. They both involve the geometry by  $\hat{\Gamma}_h^k$  and  $\Gamma_h$ , the reconstructed piecewise polynomial patches from point cloud and the triangulated original manifold, respectively. Note that  $\Gamma_h$  is just a partition of  $\Gamma$  by curved triangles of diameter  $h$ . It is common to consider piecewise Sobolev spaces for DG methods. In particular, we use the notation  $H_b^r$  to denote the broken Sobolev spaces

$$H_b^r(\hat{\Gamma}_h^k) := \left\{ v : \hat{\Gamma}_h^k \rightarrow \mathbb{R}, \text{ and } v|_{\hat{\Gamma}_h^{k,j}} \in H^r(\hat{\Gamma}_h^{k,j}), \text{ for all } j \in J \right\}, \quad (4.1)$$

where  $H^r$  denotes the standard Sobolev space, and  $r$  is the order of the differentiation. The definition in (4.1) can similarly apply to  $\Gamma$  by considering each of the corresponding curved triangles  $\Gamma_h^j$ . The finite element function space of DG method is given in an isoparametric way through parameter domain  $\Omega_h$ . Precisely we consider piecewise polynomial functions on every parametric triangle patch  $\Omega_h^j$ , which are then pulled back to the corresponding surface patches:

$$\hat{S}_h^{k,l} := \left\{ v \in L^2(\hat{\Gamma}_h^k) : v|_{\hat{\Gamma}_h^{k,j}} = \bar{v} \circ (\pi_h^k)^{-1} \text{ where } \bar{v} \in P^l(\Omega_h^j) \text{ for all } j \in J \right\}, \quad (4.2)$$

where  $l$  is the polynomial order for function values, and  $k$  is the polynomial order for reconstructing the local patches from point cloud. Again this types of spaces can also constructed for the underline exact manifold  $\Gamma_h$ , in which case, we denote by

$$S_h^l := \left\{ v \in L^2(\Gamma_h) : v|_{\Gamma_h^j} = \bar{v} \circ (\pi)^{-1} \text{ where } \bar{v} \in P^l(\Omega_h^j) \text{ for all } j \in J \right\}. \quad (4.3)$$

It is not hard to see that  $\hat{S}_h^{k,l} \subset H_b^l(\hat{\Gamma}_h^k)$  and  $S_h^l \subset H_b^l(\Gamma_h)$ , respectively. We introduce the following spaces

$$V_h^l := H^l(\Gamma_h) + H_b^l(\Gamma_h) \quad \text{and} \quad V_h^{k,l} := H^l(\hat{\Gamma}_h^k) + H_b^l(\hat{\Gamma}_h^k).$$

Their norms can characterize the DG spaces, which is often called DG norms. Here we write down the one for the former

$$\|v_h\|_{V_h^l}^2 = \sum_j \|v_h\|_{H^1(\Gamma_h^j)}^2 + \sum_{e_h \in \mathcal{E}_h} \beta_h \| [v_h] \|_{L^2(e_h)}^2 \quad \text{for every } v_h \in V_h^l.$$

The one for the latter is similar and thus omitted. For simplicity, we also denote

$$\|v_h\|_*^2 = \sum_{e_h \in \mathcal{E}_h} \beta_h \| [v_h] \|_{L^2(e_h)}^2. \quad (4.4)$$

In order to compare functions defined on  $\Gamma_h$  and  $\hat{\Gamma}_h^k$ , we rely on the pullback and pushforward operations, which are precisely defined as follows:

$$T_h^k u_h := u_h \circ \pi_h^k \circ (\pi)^{-1}. \quad (4.5)$$

Note the pullback  $T_h^k$  is a bijection and both itself and its inverse the pushforward  $(T_h^k)^{-1}$  are bounded operators in the sense that:

**Lemma 4.1.** Let  $T_h^k$  and its inverse  $(T_h^k)^{-1}$  be defined as (4.5), then

$$\|T_h^k u_h\|_{H^m(\Gamma_h)} \simeq \|u_h\|_{H^m(\hat{\Gamma}_h^k)} \quad \text{for all } 0 \leq m \leq l+1. \quad (4.6)$$

By  $a \simeq b$  we mean that there exist positive constants  $C_1$  and  $C_2$  such that  $a \leq C_1 b$  and  $b \leq C_2 a$ .

## 4.2 Laplace-Beltrami equation

To develop the convergence analysis, we follow the general strategy in [4, 13], but mostly emphasize the geometric error analysis part. It shows that the geometric error are exactly caused by the approximation of the metric tensor. We shall refer to a few lemmas from [4] on DG methods.

**Lemma 4.2** (DG trace inequality). For every  $e_h^j \in \partial\Gamma_h^j$ , and for sufficiently small  $h$ , we have

$$\|v_h\|_{L^2(e_h^j)}^2 \leq Ch^{-1} \|v_h\|_{L^2(\Gamma_h^j)}^2 \quad \text{and} \quad \|\nabla_g v_h\|_{L^2(e_h^j)}^2 \leq Ch^{-1} \|\nabla_g v_h\|_{L^2(\Gamma_h^j)}^2. \quad (4.7)$$

**Lemma 4.3** (Boundedness and coercivity of DG bilinear form). The DG bilinear form  $\mathcal{A}_h^l$  defined on  $\Gamma_h$  is bounded and coercive in DG norm provided that the stabilization parameter  $\beta$  is large enough, i.e.,

$$\mathcal{A}_h^l(u_h, v_h) \leq \|u_h\|_{V_h^l} \|v_h\|_{V_h^l} \quad \text{and} \quad \mathcal{A}_h^l(u_h, u_h) \geq C \|u_h\|_{V_h^l}^2 \quad (4.8)$$

With the above preparation, we are now ready to present our main result on the error bounds of the IPDG method.

**Theorem 4.4.** Let  $u_h^{k,l} \in \hat{S}_h^{k,l}$  be the solution by DG discretization of (2.2), and  $u \in H^{l+1}(\Gamma_h)$  is the solution of (2.1). Then we have the following quantitative convergence result:

$$\|\hat{u}_h^{k,l} - u\|_{L^2(\Gamma_h)} + h \|\hat{u}_h^{k,l} - u\|_{V_h^l} \leq Ch^{\min\{k,l\}+1} (\|f\|_{L^2(\Gamma_h)} + \|u\|_{H^{l+1}(\Gamma_h)}), \quad (4.9)$$

where  $\hat{u}_h^{k,l} = T_h^k u_h^{k,l}$  is the pullback of the function  $u_h^{k,l}$  from  $\hat{\Gamma}_h^k$  to  $\Gamma_h$ .

*Proof.* We sketch some of the major steps for a proof strategy, while highlight the part which is different to the one in [4]. We first show the estimate on the DG norm of the error  $\|\hat{u}_h^{k,l} - u\|_{V_h^l}$ .

After that we proceed with the  $L^2(\Gamma_h)$  norm error estimate.

**Step 1:** Using triangle inequality, this can be decomposed into:

$$\|\hat{u}_h^{k,l} - u\|_{V_h^l} \leq \|I_h^l u - u\|_{V_h^l} + \|I_h^l u - \hat{u}_h^{k,l}\|_{V_h^l}. \quad (4.10)$$

**Step 2:** The first term on the right hand side of (4.10) can be estimated using interpolation error estimate and the trace inequality(4.7). This gives

$$\|I_h^l u - u\|_{V_h^l} \leq Ch^l \|u\|_{H^{l+1}(\Gamma_h)}.$$

Be careful here we have interpolation both on the triangle faces and also on the edges.

**Step 3:** The second term on the right hand side of (4.10) needs a bit more work. Using the stability estimate in Lemma 4.3

$$\|I_h^l u - \hat{u}_h^{k,l}\|_{V_h^l}^2 \leq C \mathcal{A}_h^l(I_h^l u - \hat{u}_h^{k,l}, I_h^l u - \hat{u}_h^{k,l}),$$

where  $\mathcal{A}(\cdot, \cdot)$  is the bilinear forms induced by the DG discretization of the weak formulation of the PDEs, e.g., Laplace-Beltrami problem. Note that this is formulated on the underline exact manifold  $\Gamma_h$ .

**Step 4:** The key point of the proof is to estimate  $\mathcal{A}_h^l(I_h^l u - \hat{u}_h^{k,l}, I_h^l u - \hat{u}_h^{k,l})$ . Recall

$$\mathcal{A}_h^l(I_h^l u - \hat{u}_h^{k,l}, I_h^l u - \hat{u}_h^{k,l}) \leq \mathcal{A}_h^l(I_h^l u - u, I_h^l u - \hat{u}_h^{k,l}) + \mathcal{A}_h^l(u - \hat{u}_h^{k,l}, I_h^l u - \hat{u}_h^{k,l}). \quad (4.11)$$

The first term of the right hand side can be bounded by interpolation estimate and Lemma 4.3:

$$\mathcal{A}_h^l(I_h^l u - u, v_h) \leq Ch^l \|u\|_{H^{l+1}(\Gamma_h)} \|v_h\|_{V_h^l}, \quad (4.12)$$

for  $v_h \in S_h^l$ . The second term on the right-hand side of (4.11) looks like a Galerkin orthogonality residual in conformal FEM. In order to analyze it, we consider the the weak formulation and the DG approximation of the Laplace-Beltrami equation, which consists of

$$\mathcal{A}_h^l(u, v_h) = \sum_j \int_{\Gamma_h^j} f v_h dA_g$$

and

$$\mathcal{A}_h^{k,l}(u_h^{k,l}, (T_h^k)^{-1} v_h) = \sum_j \int_{\hat{\Gamma}_h^{k,j}} (T_h^k)^{-1} f (T_h^k)^{-1} v_h dA_{g_h^k},$$

where  $\mathcal{A}_h^l(\cdot, \cdot)$  and  $\mathcal{A}_h^{k,l}(\cdot, \cdot)$  denotes the DG bilinear forms on  $\Gamma_h$  and  $\hat{\Gamma}_h^k$ , respectively. Their precise forms have been given in (2.10) and (2.9).

Note that

$$\sum_j \int_{\hat{\Gamma}_h^{k,j}} (T_h^k)^{-1} f (T_h^k)^{-1} v_h dA_{g_h^k} = \sum_j \int_{\Gamma_h^j} f v_h \sigma_A dA_g,$$

where  $\sigma_A = \frac{dA_{g_h^k}}{dA_g} = \frac{\sqrt{|g_h^k|}}{\sqrt{|g|}}$ . This shows

$$\mathcal{A}_h^l(u, v_h) - \mathcal{A}_h^{k,l}(u_h^{k,l}, (T_h^k)^{-1} v_h) = \sum_j \int_{\Gamma_h^j} f v_h (1 - \sigma_A) dA_g.$$

Now we consider to calculate the quantities on the parametric domain  $\Omega_h$

$$\begin{aligned} & \mathcal{A}_h^l(T_h^k u_h^{k,l}, v_h) \\ &= \sum_j \int_{\Omega_h^j} (\nabla \bar{u}_h^{k,l})^\top g^{-1} \nabla \bar{v}_h \sqrt{|g|} dA + \beta_h \sum_{\bar{e}_h \in \bar{\mathcal{E}}_h} \int_{\bar{e}_h} [\bar{u}_h^{k,l}] [\bar{v}_h] l_g dE \\ & \quad - \sum_{\bar{e}_h \in \bar{\mathcal{E}}_h} \int_{\bar{e}_h} \left( \{(\nabla \bar{u}_h^{k,l})^\top g^{-1} \partial \pi^\top n\} [\bar{v}_h] + \{(\nabla \bar{v}_h)^\top g^{-1} \partial \pi^\top n\} [\bar{u}_h^{k,l}] \right) l_g dE \end{aligned}$$

while

$$\begin{aligned} & \mathcal{A}_h^{k,l}(u_h^{k,l}, (T_h^k)^{-1} v_h) \\ &= \sum_j \int_{\Omega_h^j} (\nabla \bar{u}_h^{k,l})^\top (g_h^k)^{-1} \nabla \bar{v}_h \sqrt{|g_h^k|} dA + \beta_h \sum_{\bar{e}_h \in \bar{\mathcal{E}}_h} \int_{\bar{e}_h} [\bar{u}_h^{k,l}] [\bar{v}_h] \{l_{g_h^k}\} dE - \\ & \quad \sum_{\bar{e}_h \in \bar{\mathcal{E}}_h} \{(\nabla \bar{u}_h^{k,l})^\top (g_h^k)^{-1} (\nabla \pi_h^k)^\top n_h\} [\bar{v}_h] l_{g_h^k} + \{(\nabla \bar{v}_h)^\top (g_h^k)^{-1} (\nabla \pi_h^k)^\top n_h\} [\bar{u}_h^{k,l}] l_{g_h^k} dE. \end{aligned}$$

We define

$$\mathcal{R}(v_h) := \mathcal{A}_h^l(u - \hat{u}_h^{k,l}, v_h). \quad (4.13)$$

which is similar but different to the Galerkin orthogonality term. We have that

$$\begin{aligned} \mathcal{R}(v_h) &= \mathcal{A}_h^{k,l}(u_h^{k,l}, (T_h^k)^{-1} v_h) - \mathcal{A}_h^l(T_h^k u_h^{k,l}, v_h) + \mathcal{A}_h^l(u, v_h) - \mathcal{A}_h^{k,l}(u_h^{k,l}, (T_h^k)^{-1} v_h) \\ &= \mathcal{A}_h^{k,l}(u_h^{k,l}, (T_h^k)^{-1} v_h) - \mathcal{A}_h^l(T_h^k u_h^{k,l}, v_h) + \sum_j \int_{\Gamma_h^j} f v_h (1 - \sigma_A) dA_g, \end{aligned}$$

which leads to

$$\begin{aligned}
\mathcal{R}(v_h) = & \sum_j \int_{\Omega_h^j} (\nabla \bar{u}_h^{k,l})^\top ((g_h^k)^{-1} - g^{-1}) \nabla \bar{v}_h \sqrt{|g_h^k|} + (\nabla \bar{u}_h^{k,l})^\top g^{-1} \nabla \bar{v}_h \left( \sqrt{|g_h^k|} - \sqrt{|g|} \right) dA \\
& - \sum_{\bar{e}_h \in \bar{\mathcal{E}}_h} \int_{\bar{e}_h} \{(\nabla \bar{u}_h^{k,l})^\top ((g_h^k)^{-1} (\nabla \pi_h^k)^\top n_h - g^{-1} (\nabla \pi)^\top n)\} [\bar{v}_h l_{g_h^k}] dE \\
& - \sum_{\bar{e}_h \in \bar{\mathcal{E}}_h} \int_{\bar{e}_h} \{(\nabla \bar{v}_h)^\top ((g_h^k)^{-1} (\nabla \pi_h^k)^\top n_h - g^{-1} (\nabla \pi)^\top n)\} [\bar{u}_h^{k,l} l_{g_h^k}] dE \\
& - \sum_{\bar{e}_h \in \bar{\mathcal{E}}_h} \int_{\bar{e}_h} \{(\nabla \bar{u}_h^{k,l})^\top g^{-1} (\nabla \pi)^\top n\} [\bar{v}_h (l_{g_h^k} - l_g)] dE \\
& - \sum_{\bar{e}_h \in \bar{\mathcal{E}}_h} \int_{\bar{e}_h} \{(\nabla \bar{v}_h)^\top g^{-1} (\nabla \pi)^\top n\} [\bar{u}_h^{k,l} (l_{g_h^k} - l_g)] dE \\
& + \beta_h \sum_{\bar{e}_h \in \bar{\mathcal{E}}_h} \int_{\bar{e}_h} [\bar{u}_h^{k,l}] [\bar{v}_h] \{ (l_{g_h^k} - l_g) \} dE + \int_{\Omega_h^j} \bar{f} \bar{v}_h \left( \sqrt{|g|} - \sqrt{|g_h^k|} \right) dA.
\end{aligned} \tag{4.14}$$

Taking into account the geometric error estimates in Proposition 3.5, each of the terms on the right-hand side of (4.14) can be estimated. The details of these estimates are given in Appendix B. To summarize all the estimates there, we derive that

$$\mathcal{R}(v_h) \leq C_1 h^{k+1} \left\| T_h^k u_h^{k,l} \right\|_{V_h^l} \|v_h\|_{V_h^l} + C_2 h^{k+1} \|f\|_{L^2(\Gamma_h)} \|v_h\|_{L^2(\Gamma_h)}, \tag{4.15}$$

Then we go back to (4.11) with (4.12)  $m = l + 1$  and (4.15) to have the statement. In order to estimate  $\left\| \hat{u}_h^{k,l} - u \right\|_{L^2(\Gamma_h)}$ , we leverage the following dual problem of (2.1):

$$-\Delta_g z + z = \hat{u}_h^{k,l} - u \quad \text{for } z \in H^2(\Gamma_h) \quad \text{and} \quad \|z\|_{H^2(\Gamma_h)} \leq C \left\| \hat{u}_h^{k,l} - u \right\|_{L^2(\Gamma_h)}. \tag{4.16}$$

Testing with  $\hat{u}_h^{k,l} - u$  on both sides gives us that

$$\left\| \hat{u}_h^{k,l} - u \right\|_{L^2(\Gamma_h)}^2 = \mathcal{A}_h^l(z, \hat{u}_h^{k,l} - u) = \mathcal{A}_h^l(\hat{u}_h^{k,l} - u, z - I_h^l z) + \mathcal{A}_h^l(\hat{u}_h^{k,l} - u, I_h^l z).$$

Then, applying standard boundedness estimate in Lemma 4.3 to the first term on the right-hand side, we have

$$\mathcal{A}_h^l(\hat{u}_h^{k,l} - u, z - I_h^l z) \leq \left\| \hat{u}_h^{k,l} - u \right\|_{V_h^l} \|z - I_h^l z\|_{V_h^l} \leq C h^{k+1} \|u\|_{H^{k+1}(\Gamma_h)} \|z\|_{H^2(\Gamma_h)}.$$

For the second term, we use the estimate from (4.15),

$$\begin{aligned}
\mathcal{A}_h^l(\hat{u}_h^{k,l} - u, I_h^l z) &= \mathcal{R}(I_h^l z) \\
&\leq C_1 h^{k+1} \left\| T_h^k u_h^{k,l} \right\|_{V_h^l} \|I_h^l z\|_{V_h^l} + C_2 h^{k+1} \|f\|_{L^2(\Gamma)} \|I_h^l z\|_{L^2(\Gamma_h)} \\
&\leq C \left( C_1 h^{k+1} \left\| T_h^k u_h^{k,l} \right\|_{V_h^l} + C_2 h^{k+1} \|f\|_{L^2(\Gamma)} \right) \|z\|_{H^2(\Gamma_h)}
\end{aligned}$$

Combining with (4.16), we end up with the expected estimates in (4.9) for the  $L^2$  norm. This concludes the proof in combination with the DG norm estimates.  $\square$

### 4.3 LB Eigenvalue problem

Let the eigenpair  $(\lambda, u)$  be the solution of the eigenvalue problem (2.3), or equivalently (2.4). The DG discretization of eigenvalue problem (2.3) can be formulated as finding pairs  $(\lambda_h^{k,l}, u_h^{k,l}) \in (\mathbb{R}, V_h^{k,l})$  such that

$$\mathcal{A}_h^{k,l}(u_h^{k,l}, v_h) = (\lambda_h^{k,l} + 1) \sum_j \int_{\Omega_h^j} \bar{u}_h^{k,l} \bar{v}_h \sqrt{|g_h^k|} dA, \quad \text{for all } v_h \in V_h^{k,l}. \tag{4.17}$$

Similarly, the discrete eigenvalues of discrete problem (4.17) can be ordered as  $0 = \lambda_{h,1}^{k,l} < \lambda_{h,2}^{k,l} \leq \dots \leq \lambda_{h,N}^{k,l}$ , and the corresponding eigenfunctions  $u_{h,i}^{k,l}$  ( $i = 1, \dots, N$ ) can be normalized as  $(u_{h,i}^{k,l}, u_{h,j}^{k,l}) = \delta_{ij}$  where  $N$  is the dimension of the DG function space.

Let  $G : L^2(\Gamma_h) \rightarrow H^1(\Gamma_h) \subset L^2(\Gamma_h)$  be the solution operator of the Laplace-Beltrami problem (2.2) which is defined as

$$\mathcal{A}(Gf, v) = (f, v), \quad \forall v \in H^1(\Gamma) \quad (4.18)$$

and  $G_h^{k,l} : L^2(\hat{\Gamma}_h^k) \rightarrow V_h^{k,l} \subset L^2(\hat{\Gamma}_h^k)$  be the discrete solution operator which is defined as

$$\mathcal{A}_h^{k,l}(G_h^{k,l} f, v_h) = ((T_h^k)^{-1} f, v_h), \quad \forall v_h \in V_h^{k,l}. \quad (4.19)$$

It is easy to see that both  $G$  and  $G_h^{k,l}$  are self-adjoint. Let  $\mu$  (or  $\mu_h^{k,l}$ ) be the eigenvalue of  $G$  (or  $G_h^{k,l}$ ). Then, we can relate the eigenvalue of (2.3) and the eigenvalue of the operator  $G$  by  $\mu = \frac{1}{1+\lambda}$ . Similarly, we have  $\mu^{k,l} = \frac{1}{1+\lambda_h^{k,l}}$ . In addition, we have

$$\lambda_h^{k,l} - \lambda = (1 + \lambda_h^{k,l})(1 + \lambda)(\mu_i - \mu_h^{k,l}). \quad (4.20)$$

The following lemma tells that the eigenvalues are invariant under geometric transformation operator  $T_h^k$  and its inverse  $(T_h^k)^{-1}$ .

**Lemma 4.5.** *If  $G\hat{v} = \mu\hat{v}$ , then  $(T_h^k)^{-1}G\hat{v} = \mu(T_h^k)^{-1}\hat{v}$ . Similarly, if  $G_h^k v_h = \mu_h^k v_h$ , then  $T_h^k G_h^k v_h = \mu_h^k T_h^k v_h$ .*

*Proof.* This is shown using the fact that the operators  $(T_h^k)^\pm$  and the scalar multiplication are commutable, i.e.,  $\mu_h^k T_h^k v_h = T_h^k \mu_h^k v_h$  and  $\mu(T_h^k)^{-1}\hat{v} = (T_h^k)^{-1}\mu\hat{v}$ .  $\square$

Using the above lemma, we have the following result.

**Lemma 4.6.** *Let  $\mu_h^{k,l}$  be an eigenvalue of the operator  $G_h^{k,l}$  on  $\hat{\Gamma}_h^k$  with eigenfunction  $u_h^{k,l}$ . Define an solution operator*

$$\tilde{G}_h^{k,l} := T_h^k G_h^{k,l} (T_h^k)^{-1} \quad \text{on } \Gamma_h. \quad (4.21)$$

*Then  $\mu_h^{k,l}$  is an eigenvalue of  $\tilde{G}_h^{k,l}$  and the corresponding eigenfunction is  $(T_h^k)^{-1}u_h^{k,l}$ .*

*Proof.* Let  $\hat{u}_h^{k,l} := T_h^k u_h^{k,l}$ . Notice that  $G_h^{k,l} u_h^{k,l} = \mu_h^{k,l} u_h^{k,l}$  which implies that  $G_h^k (T_h^k)^{-1} \hat{u}_h^{k,l} = \mu_h^k (T_h^k)^{-1} \hat{u}_h^{k,l} = (T_h^k)^{-1} \mu_h^k \hat{u}_h^{k,l}$ . It tells that  $T_h^k G_h^k (T_h^k)^{-1} \hat{u}_h^{k,l} = \mu_h^k \hat{u}_h^{k,l}$ , which completes the proof.  $\square$

To simplify the notation, we define

$$\mathcal{E}_h^{k,l}(G) := G - \tilde{G}_h^{k,l}. \quad (4.22)$$

Using Theorem 4.4 for the source problem, we can show the operator approximation result

**Lemma 4.7.** *Let  $\tilde{G}_h^{k,l} : L^2(\Gamma_h) \rightarrow V_h^l \subset L^2(\Gamma_h)$  be defined as in (4.21), and  $\mathcal{E}_h^{k,l}(G)$  be given as (4.22). Then the following approximation properties hold:*

$$\left\| \mathcal{E}_h^{k,l}(G) \right\|_{\mathcal{L}(L^2(\Gamma_h))} = \mathcal{O}(h^{\min\{k,l\}+1}). \quad (4.23)$$

In particular, we have

$$\lim_{h \rightarrow 0} \left\| \mathcal{E}_h^{k,l}(G) \right\|_{\mathcal{L}(L^2(\Gamma_h))} \rightarrow 0. \quad (4.24)$$

Let  $\rho(G)$  (or  $\rho(\tilde{G}_h^{k,l})$ ) denote the resolvent set of operator  $G$  (or  $\tilde{G}_h^{k,l}$ ), and  $\sigma(G)$  (or  $\sigma(\tilde{G}_h^{k,l})$ ) denote the spectrum set of operator  $G$  (or  $\tilde{G}_h^{k,l}$ ). We define the spectral projection operator

$$E(\mu) := \frac{1}{2\pi i} \int_{\gamma} (z - G)^{-1} dz.$$

Here  $\gamma \subset \rho(G)$  is a curve in the complex domain which encloses  $\mu \in \sigma(G)$  but no other eigenvalues of  $G$ . Let  $R(E)$  denote the range of  $E$ . Let  $\mu$  be an eigenvalue of the operator  $G$ , and it has algebraic multiplicity  $m$ . Then, combining Theorem 9.1 in [8] and (4.24) implies that no pollution of the spectrum, i.e.  $\gamma$  encloses exactly  $m$  discrete eigenvalues  $\left\{ \mu_{h,i}^{k,l} \right\}_{i=1}^m$  of  $\tilde{G}_h^{k,l}$  approximating  $\mu$ .

Using the Babuška-Osborn spectral approximation theory [7], we have the following convergence results on eigenvalues and eigenfunctions.

**Theorem 4.8.** Let  $\mu_h^{k,l}$  be an eigenvalue converging to  $\mu$ . Let  $\hat{u}_h^{k,l}$  be a unit eigenfunction of  $\tilde{G}_h^{k,l}$  associated with the eigenvalue  $\mu_h^{k,l}$ . Then there exists a unit eigenvector  $u \in R(E)$  such that the following estimates hold

$$\|u - \hat{u}_h^{k,l}\|_{L^2(\Gamma_h)} \leq Ch^{\min\{k,l\}+1}, \quad (4.25)$$

$$|\mu - \mu_h^{k,l}| \leq C(\lambda)(h^{\min\{k+1,2l\}}), \quad (4.26)$$

$$|\lambda - \lambda_h^{k,l}| \leq C(\lambda)(h^{\min\{k+1,2l\}}), \quad (4.27)$$

where  $l \geq 1$  and  $k \geq 1$  are orders of the local polynomials for function and geometry approximations, respectively.

*Proof.* For the eigenfunction approximation, Theorem 7.4 in [7] and the approximation property (4.23) already imply that

$$\|u - \hat{u}_h^{k,l}\|_{L^2(\Gamma_h)} \leq \|\mathcal{E}_h^{k,l}(G)|_{R(E)}\|_{L^2(\Gamma_h)} \leq Ch^{\min\{k,l\}+1}. \quad (4.28)$$

To establish the eigenvalue approximation result (4.26), we apply Theorem 7.3 in [7]. Let  $v_1, \dots, v_m$  be any orthonormal basis for  $R(E)$ . Then, Theorem 7.3 in [7] implies that there exists a constant  $C$  such that

$$|\mu - \mu_h| \leq C \sum_{j,k=1}^m |(\mathcal{E}_h^{k,l}(G)v_j, v_k)| + C\|\mathcal{E}_h^{k,l}(G)|_{R(E)}\|_{L^2(\Gamma_h)}^2. \quad (4.29)$$

The second term can be bounded by  $\mathcal{O}(h^{2\min\{k,l\}+2})$ . For the first term, we have

$$\begin{aligned} & (\mathcal{E}_h^{k,l}(G)v_j, v_k) \\ &= \mathcal{A}(Gv_j, Gv_k) - \mathcal{A}_h^l(\tilde{G}_h^{k,l}v_j, \tilde{G}_h^{k,l}v_k) + \mathcal{A}_h^l(\tilde{G}_h^{k,l}v_j, \tilde{G}_h^{k,l}v_k) - (\tilde{G}_h^{k,l}v_j, v_k). \end{aligned} \quad (4.30)$$

Now we estimate each of the two paired terms on the right hand side of (4.30) individually. The first one gives

$$\begin{aligned} \mathcal{A}(Gv_j, Gv_k) - \mathcal{A}_h^l(\tilde{G}_h^{k,l}v_j, \tilde{G}_h^{k,l}v_k) &= \mathcal{A}_h^l(Gv_j, Gv_k) - \mathcal{A}_h^l(\tilde{G}_h^{k,l}v_j, \tilde{G}_h^{k,l}v_k) \\ &= \mathcal{A}_h^l(Gv_j - \tilde{G}_h^{k,l}v_j, Gv_k) + \mathcal{A}_h^l(\tilde{G}_h^{k,l}v_j, Gv_k - \tilde{G}_h^{k,l}v_k) \\ &= \mathcal{A}_h^l(\mathcal{E}_h^{k,l}(G)v_j, \tilde{G}_h^{k,l}v_k) + \mathcal{A}_h^l(\tilde{G}_h^{k,l}v_j, \mathcal{E}_h^{k,l}(G)v_k) + \mathcal{A}_h^l(\mathcal{E}_h^{k,l}(G)v_j, \mathcal{E}_h^{k,l}(G)v_k), \end{aligned} \quad (4.31)$$

where the first equality holds since  $Gv_j, Gv_k \in H^2(\Gamma_h)$  are continuous for two dimensional  $\Gamma_h$ . Notice that the third term on the last line of (4.31) can be easily estimated by

$$\mathcal{A}_h^l(\mathcal{E}_h^{k,l}(G)v_j, \mathcal{E}_h^{k,l}(G)v_k) \leq \|\mathcal{E}_h^{k,l}(G)v_j\|_{V_h^l} \|\mathcal{E}_h^{k,l}(G)v_k\|_{V_h^l}.$$

While for the first and the second terms on last line of (4.31), we recall to (4.13), which then indicates the following

$$\mathcal{A}_h^l(\mathcal{E}_h^{k,l}(G)u, \tilde{G}_h^{k,l}v) + \mathcal{A}_h^l(\tilde{G}_h^{k,l}u, \mathcal{E}_h^{k,l}(G)v) \leq \mathcal{R}(\tilde{G}_h^{k,l}v) + \mathcal{R}(\tilde{G}_h^{k,l}u) \leq Ch^{k+1},$$

where  $\mathcal{R}(\cdot)$  is defined in (4.13) and estimated in (4.15).

For the second term on the right hand side of (4.30), we have

$$\begin{aligned} & |\mathcal{A}_h^l(\tilde{G}_h^{k,l}u, \tilde{G}_h^{k,l}v) - (\tilde{G}_h^{k,l}u, v)| \\ & \leq |\mathcal{A}_h^l(\tilde{G}_h^{k,l}u, \tilde{G}_h^{k,l}v) - \mathcal{A}_h^l(G_h^{k,l}T_h^k u, G_h^{k,l}T_h^k v) + \mathcal{A}_h^l(G_h^{k,l}T_h^k u, G_h^{k,l}T_h^k v) - (G_h^{k,l}T_h^k u, T_h^k v)| \\ & \quad + |(G_h^{k,l}T_h^k u, T_h^k v) - (\tilde{G}_h^{k,l}u, v)| \\ & \leq Ch^{k+1} + \underbrace{|\mathcal{A}_h^l(G_h^{k,l}T_h^k u, G_h^{k,l}T_h^k v) - (G_h^{k,l}T_h^k u, T_h^k v)|}_{=0} + Ch^{k+1}, \end{aligned}$$

where the first and the third terms are due to the geometric error estimates from Proposition 3.5. Summarizing the above estimates, it concludes the proof of (4.25). (4.27) is a direct consequence of (4.26) and (4.20).  $\square$

**Remark 4.9.** Note that the conclusion of Theorem 4.8 and its proof can also be applied to continuous Galerkin method on surfaces. We notice here that the geometric approximation error and the function discretization error are not in the same order for higher-order element cases for the eigenvalue approximation, i.e., the convergence rates of order  $\mathcal{O}(h^{\min\{2l, 2k\}})$ , which was observed in some numerical cases in [10]. In fact, the above error estimates turn out to be theoretically sharp given the geometric approximation error and the function approximation error there. To see this, we consider an example on unit sphere  $\Gamma$ . Let the approximation manifold be another sphere  $\hat{\Gamma}_h^k$  with radius  $1 + h^{k+1}$ , which satisfies the geometric approximation error  $\|\pi - \pi_h^k\| \leq h^{k+1}$ . Now we consider the Laplace-Beltrami operator on  $\hat{\Gamma}_h^k$  and its eigenvalues. Using the analytical formula of sphere harmonics, we know that the eigenvalues associated to  $\hat{\Gamma}_h^k$  are of the following form  $\lambda_h^k \in \left(\frac{n(n+1)}{(1+h^{k+1})}\right)_{n=1}^{\infty}$ , while for  $\Gamma$  are  $\lambda \in (n(n+1))_{n=1}^{\infty}$ . Therefore the error is  $|\lambda - \lambda_h^k| = \frac{n(n+1)h^{k+1}}{(1+h^{k+1})}$ . This shows even in this ideal case, the eigenvalues' approximation error of order  $h^{2k}$  can not be achieved in general for geometric approximation error only of order  $\mathcal{O}(h^{k+1})$  when  $k > 1$ . This could serve as an intuitive example.

## 5 Numerical results

In the following, we present a series of benchmark numerical experiments to verify our theoretical findings on the error analysis of the proposed DG method on point clouds. We pick two representative manifolds, the unit sphere and a torus surface, which have genus zero and one, respectively. Before going to numerical results of the optimal convergence rates of the DG method for solving both source and eigenvalue problems of LB operator on point clouds, we first provide a validation of the geometric error bounds of Algorithm 1.

### 5.1 Geometric error

To simplify the presentation, we introduce the following notations

$$e_n^k = \max_{i \in N} |\psi^i - \xi^i|, \quad \text{and} \quad e_t^k = \max_{i \in N} |\psi_{\Omega}^i - \xi_{\Omega}^i|,$$

where the superscript  $k$  denotes the  $k$ th order polynomials used in the patch reconstruction from point cloud, and  $N$  represents the number of nodal points of  $\Omega_h$ .

We first check the accuracy claimed for Algorithm 1 based on point cloud which is sampled from the unit sphere and is uniform distributed on its spherical coordinate. In the first test, the initial mesh is generated using CGAL [2] whose vertices are  $\mathcal{O}(h^2)$  to the unit sphere. In practice, such meshes can be generated using Poisson surface reconstruction [24] which is available in the computational geometry algorithm library CGAL [2]. To depict the convergence rates, we conduct a uniform refinement for each triangle by dividing into four similar subtriangles. A main difference between the classical refinement for surface finite element methods [14] is that we do not ask for the precise embedding of submanifolds, e.g., the level set functions or parameterization functions. Note that Assumption 3.1 holds already due to the interpolation of the mesh in this example. For the general case, we can adjust the vertices of the mesh using the point cloud reconstruction before proceeding uniform refinements, and this costs no extra work.

To assess the result of Proposition 3.5, we report the difference between the reconstructed nodal points and the exact nodal ones in Table 1. Due to the structure of the sphere, the exact nodal points are obtained by stretching the reconstructed nodes along with radial directions. Note that the error bounds of  $\mathcal{O}(h^{k+1})$  can be observed except outliers. We also list the errors after projecting the paired nodal points onto the parametric domain  $\Omega_h$  in Table 2, which illustrates the  $\mathcal{O}(h^{k+2})$  convergence rate. These ally with the theoretical results established in Proposition 3.5.

Notice that, in the sphere case, surprisingly, we can observe some geometric superconvergence phenomenon in the reconstructed patches when the even-order polynomial is employed like quadratic and quartic polynomials. This implies the superconvergence geometric approximation results in the eigenvalue problem later.

Another set of tests are implemented with point cloud presentation of a torus surface:

$$\begin{cases} x = (4 \cos(\theta) + 1) \cos(\phi), \\ y = (4 \cos(\theta) + 1) \sin(\phi), \\ z = 4 \sin(\theta). \end{cases} \quad (5.1)$$

Table 1: Errors of patch reconstruction from point cloud on unit sphere

$N_v$	$e_n^1$	Order	$e_n^2$	Order	$e_n^3$	Order	$e_n^4$	Order
222	1.12e-02	—	1.52e-05	—	1.35e-05	—	9.02e-08	—
882	2.95e-03	1.94	1.09e-05	0.47	2.68e-06	2.34	4.27e-08	1.09
3522	7.21e-04	2.03	7.14e-07	3.94	9.42e-08	4.84	3.40e-10	6.98
14082	1.80e-04	2.00	4.65e-08	3.94	4.83e-09	4.29	3.56e-12	6.58
56322	4.64e-05	1.96	3.77e-09	3.62	4.07e-10	3.57	1.22e-13	4.87

Table 2: Decomposed error in the parametric domain for sphere point cloud

$N_v$	$e_t^1$	Order	$e_t^2$	Order	$e_t^3$	Order	$e_t^4$	Order
222	3.88e-04	—	1.63e-05	—	1.16e-05	—	1.44e-07	—
882	1.71e-03	-2.15	1.81e-05	-0.16	5.19e-06	1.16	1.15e-07	0.33
3522	2.13e-04	3.01	5.92e-07	4.94	1.61e-07	5.01	9.09e-10	6.99
14082	2.69e-05	2.98	1.91e-08	4.96	5.41e-09	4.90	8.15e-12	6.80
56322	3.47e-06	2.96	7.04e-10	4.76	2.37e-10	4.51	9.61e-14	6.41

The point cloud is generated from uniformly distributed points in  $(\theta, \phi)$  coordinate and then projected onto the torus.

In Table 3, we present the numerical error for the reconstructed nodal points as the first example. We can observe error bounds of order  $\mathcal{O}(h)^{k+1}$  when  $k$ th order polynomials are used. Similarly,  $\mathcal{O}(h^{k+2})$  error bounds for the nodal pairs projected onto the parameter domain coincide with Proposition 3.5. Different from the unit sphere case, there seems no geometrical superconvergence for even polynomials, different to the previous example.

Table 3: Errors of patch reconstruction from point cloud on torus

$N_v$	$e_n^1$	Order	$e_n^2$	Order	$e_n^3$	Order	$e_n^4$	Order
200	4.67e-02	—	1.66e-03	—	3.17e-04	—	6.63e-05	—
800	1.44e-02	1.69	7.79e-04	1.09	8.62e-05	1.88	9.45e-06	2.81
3200	3.39e-03	2.09	5.81e-05	3.75	2.54e-06	5.08	1.98e-07	5.58
12800	9.00e-04	1.91	5.81e-06	3.32	1.15e-07	4.47	3.92e-09	5.66
51200	2.48e-04	1.86	1.09e-06	2.42	7.06e-09	4.02	1.14e-10	5.11

Table 4: Decomposed error in the parametric domain for point cloud on torus

$N_v$	$e_t^1$	Order	$e_t^2$	Order	$e_t^3$	Order	$e_t^4$	Order
200	2.92e-03	—	1.37e-03	—	3.48e-04	—	7.41e-05	—
800	1.67e-02	-2.52	1.85e-03	-0.43	2.22e-04	0.65	4.04e-05	0.88
3200	2.46e-03	2.77	1.25e-04	3.89	7.83e-06	4.82	6.07e-07	6.06
12800	3.17e-04	2.95	8.34e-06	3.90	2.46e-07	4.99	1.32e-08	5.53
51200	4.34e-05	2.87	6.82e-07	3.61	8.29e-09	4.89	2.42e-10	5.76

## 5.2 PDEs on point cloud of the unit sphere

Now we show the numerical results of the proposed DG method for discretizing Laplace-Beltrami operator on the point cloud generated patches. We first give results for the Laplace-Beltrami equation (2.1). The right hand side function  $f(x)$  is chosen to fit the exact solution  $u(x) = x_1 x_2$ . In this test, we choose the finite element degree  $l$  and the geometric degree  $k$  equal to some  $p$  for  $p \in \{1, 2, 3, 4\}$ . According to the Theorem 4.4, we would expect  $\mathcal{O}(\max\{h^{l+1}, h^{k+1}\})$  for  $L_2$  error and  $\mathcal{O}(\max\{h^l, h^k\})$  convergence for  $H^1$  error for sufficiently small  $h$ . Without causing confusion, we use  $e^p$  (or  $De^p$ ) to denote the  $L^2$  (or  $H^1$ ) error with  $p$ th order degree. The numerical results are plotted in Figure 1, where optimal convergence rates can be observed as desired.

Then we test with the DG discretizing of the Laplace-Beltrami eigenvalue problem (2.3) using the same surface patches. For the Laplace-Beltrami operator on the unit sphere, eigenvalues and

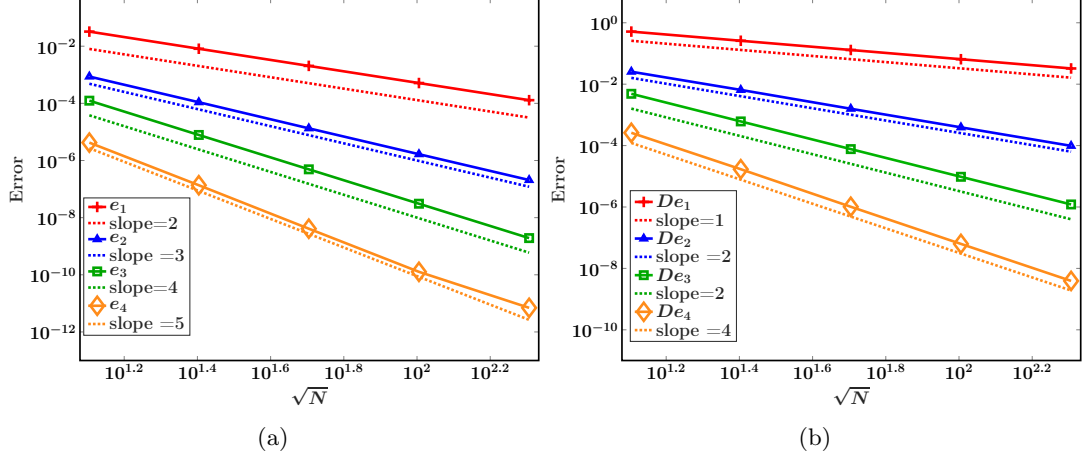


Figure 1: Numerical results of Laplace-Beltrami equation on the unit sphere. (a):  $L_2$  error; (b):  $H_1$  error.

eigenfunctions are known explicitly. In the experiments, we focus on the computation of the first nonzero eigenvalue  $\lambda_2 = \lambda_3 = \lambda_4 = 2$ . The corresponding eigenfunctions are  $u_i = x_{i-1}$  for  $i = 2, 3, 4$ , which are called spherical harmonics [1].

According to Theorem 4.8, the eigenvalue  $\lambda_i$  converges optimally at the rate of  $\mathcal{O}(\max\{h^{2l}, h^{k+1}\})$ . Taking  $l = 2$  as example, we need  $k = 3$  to observe the optimal convergence. The corresponding numerical results are reported in Table 5, where the expected rates can be observed.

Table 5: Numerical result of Laplace-Beltrami eigenvalue problem on the unit sphere point cloud when  $l = 2$  and  $k = 3$

i	$N_v$	$ \lambda_i - \lambda_{i,h} $	Order	$\ u_i - u_{i,h}\ _{0,\Gamma_h}$	Order	$ u_i - u_{i,h} _{1,\Gamma_h}$	Order
2	222	3.99e-05	—	4.20e-04	—	1.07e-02	—
2	882	2.82e-06	3.84	5.26e-05	3.01	2.72e-03	1.99
2	3522	1.81e-07	3.97	6.59e-06	3.00	6.83e-04	1.99
2	14082	1.16e-08	3.97	8.27e-07	3.00	1.72e-04	1.99
3	222	5.18e-05	—	4.28e-04	—	1.09e-02	—
3	882	3.50e-06	3.91	5.37e-05	3.01	2.76e-03	1.99
3	3522	2.25e-07	3.97	6.74e-06	3.00	6.94e-04	1.99
3	14082	1.43e-08	3.98	8.45e-07	3.00	1.74e-04	1.99
4	222	6.52e-05	—	4.45e-04	—	1.12e-02	—
4	882	4.38e-06	3.92	5.58e-05	3.01	2.85e-03	1.99
4	3522	2.79e-07	3.97	6.98e-06	3.00	7.17e-04	1.99
4	14082	1.77e-08	3.98	8.75e-07	3.00	1.80e-04	1.99

We also test for other choice of  $k$  and  $l$ . The numerical results for  $l = 3$  and  $k = 4$  are documented in Table 6. According to Theorem 4.8, we would only expect  $\mathcal{O}(h^5)$  order convergence in the eigenvalues. However, interestingly,  $\mathcal{O}(h^6)$  order convergence is observed for the eigenvalue, which is due to the superconvergence of the geometric approximation reported in the previous section. To further demonstrate this, we test the case  $k = l = 2$ . The numerical output are reported in Table 7. Again, improved convergence rates are observed, which support the error bounds  $\mathcal{O}(\max\{h^{2l}, h^{k+2}\})$  when  $k$  is even. Surprisingly, we also observe the  $\mathcal{O}(h^{k+2})$  (or  $\mathcal{O}(h^{k+1})$ ) order superconvergence for eigenfunctions' approximation in  $L^2$  norm (or  $H^1$  norm).

Table 6: Numerical result of Laplace-Beltrami eigenvalue problem on the unit sphere point cloud when  $l = 3$  and  $k = 4$

i	$N_v$	$ \lambda_i - \lambda_{i,h} $	Order	$\ u_i - u_{i,h}\ _{0,\Gamma_h}$	Order	$ u_i - u_{i,h} _{1,\Gamma_h}$	Order
2	222	1.46e-08	—	2.00e-05	—	7.08e-04	—
2	882	8.98e-10	4.04	1.33e-06	3.92	9.35e-05	2.93
2	3522	1.59e-11	5.82	8.01e-08	4.06	1.14e-05	3.04
2	14082	1.69e-11	-0.08	4.59e-09	4.13	1.34e-06	3.09
3	222	3.15e-08	—	1.97e-05	—	6.95e-04	—
3	882	1.21e-09	4.72	1.19e-06	4.07	8.52e-05	3.04
3	3522	1.73e-11	6.14	7.84e-08	3.93	1.11e-05	2.94
3	14082	2.10e-11	-0.28	4.72e-09	4.06	1.36e-06	3.03
4	222	4.84e-08	—	1.77e-05	—	6.39e-04	—
4	882	1.48e-09	5.06	1.22e-06	3.87	8.75e-05	2.88
4	3522	1.88e-11	6.31	7.12e-08	4.11	1.04e-05	3.08
4	14082	3.30e-11	-0.82	4.97e-09	3.84	1.41e-06	2.88

Table 7: Numerical result of Laplace-Beltrami eigenvalue problem on the unit sphere when  $k = 2$  and  $l = 2$

i	$N_v$	$ \lambda_i - \lambda_{i,h} $	Order	$\ u_i - u_{i,h}\ _{0,\Gamma_h}$	Order	$ u_i - u_{i,h} _{1,\Gamma_h}$	Order
2	222	1.09e-04	—	2.12e-05	—	1.21e-03	—
2	882	7.65e-06	3.86	3.58e-06	2.58	4.83e-04	1.33
2	3522	4.67e-07	4.04	2.16e-07	4.06	6.08e-05	3.00
2	14082	2.92e-08	4.00	1.34e-08	4.01	7.62e-06	3.00
3	222	1.22e-04	—	2.42e-05	—	1.20e-03	—
3	882	8.28e-06	3.90	3.86e-06	2.66	4.90e-04	1.30
3	3522	5.14e-07	4.02	2.35e-07	4.04	6.16e-05	3.00
3	14082	3.22e-08	4.00	1.46e-08	4.00	7.72e-06	3.00
4	222	1.44e-04	—	2.77e-05	—	1.18e-03	—
4	882	9.94e-06	3.88	4.58e-06	2.61	4.99e-04	1.25
4	3522	6.11e-07	4.03	2.74e-07	4.07	6.27e-05	3.00
4	14082	3.81e-08	4.00	1.69e-08	4.02	7.86e-06	3.00

### 5.3 PDEs on point cloud of a torus

In the following, we present numerical solutions of the DG method on the patches reconstructed from the torus point cloud. Similar to the last example, we start with the Laplace-Beltrami equation (2.1). The cooked up exact solution is  $u(x) = x_1 - x_2$  and then the right hand side function  $f(x)$  can be simply computed. We set  $k = l = p$  for some  $p = 1, \dots, 4$ . The numerical errors are documented in Figure 2. From there we can spot the optimal convergence rates for both  $L^2$  and  $H^1$  errors.

For the comparison of eigenvalues for the LB operator, it is different to the unit sphere case, as the exact eigenvalues of LB operator on torus are not known to us. In order to study the convergence rates, we use the following relative error

$$Err_i = \frac{|\lambda_{i,h_{j+1}} - \lambda_{i,h_j}|}{\lambda_{i,h_{j+1}}}, \quad (5.2)$$

where  $h_j$  is the mesh-size on the  $j$ th level of meshes. The numerical results are reported in Figure 3a for  $k = l = 2$ . We compare the first five nontrivial eigenvalues. What stands out in this figure is that 4th order convergence is shown up, which seems indicate  $\mathcal{O}(\max\{h^{2l}, h^{k+2}\})$  bounds for eigenvalue approximation when  $k$  is even. In Figure 3b, we display the eigenvalue approximation

error when  $k = l = 4$ . Superconvergence of the geometric approximations are presented again in both the even-order polynomial cases. This kind of superconvergence results may deserve further investigation.

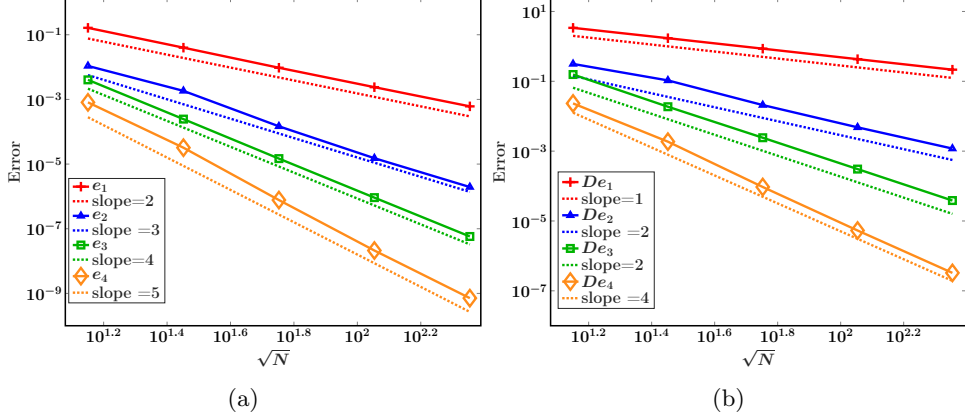


Figure 2: Numerical results of Laplace-Beltrami equation on torus point could. (a):  $L_2$  error; (b):  $H_1$  error.

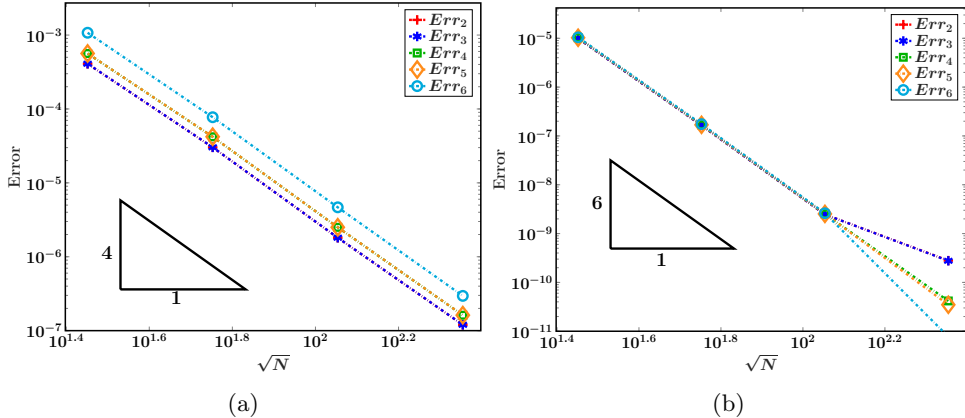


Figure 3: Numerical results of Laplace-Beltrami eigenvalue problem on torus point cloud. (a):  $k = l = 2$ ; (b):  $k = l = 4$ .

## 6 Conclusion

In this paper, we have proposed a DG method for numerical solutions of PDEs on point clouds. Our particular focus is on the numerical analysis of this method since existing results in the literature are not applicable in such a case. To do so, we introduced a new error analysis framework for the geometric approximation without embedding and global continuity assumptions. This framework provides a common umbrella to cover existing numerical analysis results on surface Galerkin methods (including both continuous and discontinuous finite elements) in the literature, even though it is implemented for a specific DG method only.

## A A proof of Lemma 3.2

*Proof.* We consider first the case that  $p_h^{k,j}$  is produced from interpolation by the polynomial graph, let us denote by  $p_h^{*,k,j}$ . This is when the number  $m$  in calculating (3.1) in Algorithm 1 equals to the number of unknown coefficients for determining the polynomial, let us denote it by  $m^*$ . Then the

above estimate is a direct result from approximation theory. When  $m > m*$ , we use the property that  $p_h^{k,j}$  is a minimizer of (3.1). It is evident that

$$\sum_{i=1}^m |p^j(r_i^j) - p_h^{k,j}(r_i^j)|^2 \leq \sum_{i=1}^m |p^j(r_i^j) - p_h^{*k,j}(r_i^j)|^2,$$

since  $p^j(r_i^j) = \zeta_i^j$  for  $i = 1, \dots, m$ . We have  $|p^j(r_i^j) - p_h^{*k,j}(r_i^j)| \leq Ch^{k+1}$  for all  $i = 1, \dots, m$ , which indicates that

$$|p^j(r_i^j) - p_h^{k,j}(r_i^j)| \leq C'h^{k+1} \text{ for all } i = 1, \dots, m.$$

We have also that  $p_h^{*k,j}$  interpolates  $p^j$ . As  $p_h^{*k,j}$  and  $p_h^{k,j}$  both be  $k^{th}$  order local polynomials. Then we can pick  $m*$  points out of the  $m$  points, and to have  $p_h^{k,j} = \sum_i^{m*} p_h^{k,j}(r_i^j) \phi_i$ , and  $p_h^{*k,j} = \sum_i^{m*} p^j(r_i^j) \phi_i$ , where  $(\phi_i)_{i=1}^{m*}$  are Lagrange polynomial bases. Since  $|p_h^{*k,j}(r_i^j) - p_h^{k,j}(r_i^j)| \leq Ch^{k+1}$ , and  $|\phi_i| \leq C$  due to our assumption on the distribution of the selected reconstruction points. We have then for all  $r \in \Omega_h^j$

$$|p_h^{*k,j}(r) - p_h^{k,j}(r)| \leq \sum_{i=1}^{m*} |\phi_i(r)| |p_h^{*k,j}(r_i^j) - p_h^{k,j}(r_i^j)| \leq Ch^{k+1}.$$

This gives us the estimate using the triangle inequality

$$|p^j(r) - p_h^{k,j}(r)| \leq |p^j(r) - p_h^{*k,j}(r)| + |p_h^{*k,j}(r) - p_h^{k,j}(r)| = \mathcal{O}(h^{k+1}) \quad \text{for all } r \in \Omega_h^j.$$

Finally, standard argument leads to the estimate on the derivatives (gradient):

$$|\nabla p^j(r) - \nabla p_h^{k,j}(r)| = \mathcal{O}(h^k) \quad \text{for all } r \in \Omega_h^j.$$

□

## B Details on the estimate for each terms in (4.14)

Note that the results of Proposition 3.5 are crucial for the estimates here. For the first term in (4.14), we have:

$$\begin{aligned} & \sum_j \int_{\Omega_h^j} (\nabla \bar{u}_h^{k,l})^\top ((g_h^k)^{-1} - g^{-1}) \nabla \bar{v}_h \sqrt{|g_h^k|} + (\nabla \bar{u}_h^{k,l})^\top g^{-1} \nabla \bar{v}_h \left( \sqrt{|g_h^k|} - \sqrt{|g|} \right) dA \\ & \leq \|g_h^k ((g_h^k)^{-1} - g^{-1})\|_{L^\infty} \left| \sum_j \int_{\Omega_h^j} (\nabla \bar{u}_h^{k,l})^\top (g_h^k)^{-1} \nabla \bar{v}_h \sqrt{|g_h^k|} dA \right| + \\ & \quad \left\| \left( \sqrt{|g_h^k|} - \sqrt{|g|} \right) \sqrt{|g|}^{-1} \right\|_{L^\infty} \left| \sum_j \int_{\Omega_h^j} (\nabla \bar{u}_h^{k,l})^\top g^{-1} \nabla \bar{v}_h \sqrt{|g|} dA \right| \\ & \leq Ch^{k+1} \left( \|u_h^{k,l}\|_{H^1(\hat{\Gamma}_h^k)} \| (T_h^k)^{-1} v_h \|_{H^1(\hat{\Gamma}_h^k)} + \|T_h^k u_h^{k,l}\|_{H^1(\Gamma_h)} \|v_h\|_{H^1(\Gamma_h)} \right) \\ & = \mathcal{O}(h^{k+1}) \|T_h^k u_h^{k,l}\|_{V_h^l} \|v_h\|_{V_h^l}, \end{aligned}$$

where the last inequality is due to the equivalence of the norms of  $H^1(\hat{\Gamma}_h^k)$  and  $H^1(\Gamma_h)$  and the embedding that  $H^1(\Gamma_h) \subset V_h^l$ . For the second term, we have

$$\begin{aligned} & - \sum_{\bar{e}_h \in \bar{\mathcal{E}}_h} \int_{\bar{e}_h} \{(\nabla \bar{u}_h^{k,l})^\top ((g_h^k)^{-1} (\nabla \pi_h^k)^\top n_h - g^{-1} (\nabla \pi)^\top n)\} [\bar{v}_h] l_{g_h^k} dE \\ & \leq \left\| \frac{l_{g_h^k}}{l_g} \right\|_{L^\infty} \| ((g_h^k)^{-1} (\nabla \pi_h^k)^\top n_h - g^{-1} (\nabla \pi)^\top n) \|_{L^\infty} \left| \sum_{\bar{e}_h \in \bar{\mathcal{E}}_h} \int_{\bar{e}_h} \{(\nabla \bar{u}_h^{k,l})^\top\} [\bar{v}_h] l_g dE \right| \\ & \leq Ch^{k+1} \left\| \sqrt{\beta_h}^{-1} \nabla_g T_h^k u_h^{k,l} \right\|_{L^2(\partial \Gamma_h)} \left\| \sqrt{\beta_h} v_h \right\|_{L^2(\partial \Gamma_h)} \\ & = \mathcal{O}(h^{k+1}) \|T_h^k u_h^{k,l}\|_{H^1(\Gamma_h)} \|v_h\|_* = \mathcal{O}(h^{k+1}) \|T_h^k u_h^{k,l}\|_{V_h^l} \|v_h\|_{V_h^l}. \end{aligned}$$

while the second last relation we used Cauchy-Schwartz inequality, Lemma 4.2, the norm defined in (4.4) and the relation that  $\beta_h = \frac{\beta}{h}$ . Similarly, for the third term

$$\begin{aligned} & - \sum_{\bar{e}_h \in \mathcal{E}_h} \int_{\bar{e}_h} \{(\nabla \bar{v}_h)^\top ((g_h^k)^{-1} (\nabla \pi_h^k)^\top n_h - g^{-1} (\nabla \pi)^\top n)\} [\bar{u}_h^{k,l} l_{g_h^k}] dE \\ & = \mathcal{O}(h^{k+1}) \|v_h\|_{H^1(\Gamma_h)} \|T_h^k u_h^{k,l}\|_* = \mathcal{O}(h^{k+1}) \|v_h\|_{V_h^l} \|T_h^k u_h^{k,l}\|_{V_h^l}. \end{aligned}$$

The fourth and the fifth term are also quite similar, while we only have to take care of the geometric error contributed by  $\|l_{g_h^k} - l_g\|_{L^\infty}$  then we will end up with the same estimate of the second and the third ones up to different constants. The rest two terms are also quite trivial and we omit the details.

## Acknowledgment

Guozhi Dong was supported by the Deutsche Forschungsgemeinschaft (DFG, German Research Foundation) under Germany's Excellence Strategy – The Berlin Mathematics Research Center MATH+ (EXC-2046/1, project ID: 390685689). Hailong Guo was partially supported by Andrew Sisson Fund of the University of Melbourne. Zuoqiang Shi was supported by NSFC Grant 12071244.

## References

- [1] M. Abramowitz and I. A. Stegun. *Handbook of mathematical functions with formulas, graphs, and mathematical tables*, volume 55 of *National Bureau of Standards Applied Mathematics Series*. For sale by the Superintendent of Documents, U.S. Government Printing Office, Washington, D.C., 1964.
- [2] P. Alliez, L. Saboret, and G. Guennebaud. Poisson surface reconstruction. In *CGAL User and Reference Manual*. CGAL Editorial Board, 5.1.1 edition, 2020.
- [3] P. F. Antonietti, A. Buffa, and I. Perugia. Discontinuous Galerkin approximation of the Laplace eigenproblem. *Comput. Methods Appl. Mech. Engrg.*, 195:3483–3503, 2006.
- [4] P. F. Antonietti, A. Dedner, P. Madhavan, S. Stangalino, B. Stinner, and M. Verani. High order discontinuous Galerkin methods for elliptic problems on surfaces. *SIAM J. Numer. Anal.*, 53(2):1145–1171, 2015.
- [5] D.N. Arnold. An interior penalty finite element method with discontinuous elements. *SIAM J. Numer. Anal.*, 19:742–760, 1982.
- [6] T. Aubin. Best constants in the Sobolev imbedding theorem: the Yamabe problem. In *Seminar on Differential Geometry*, volume 102 of *Ann. of Math. Stud.*, pages 173–184. Princeton Univ. Press, Princeton, N.J., 1982.
- [7] I. Babuška and J. Osborn. *Eigenvalue problems*, volume II of *Handbook of Numerical Analysis*. North-Holland, Amsterdam, 1991.
- [8] D. Boffi. Finite element approximation of eigenvalue problems. *Acta Numerica*, 2010:1–120, 2010.
- [9] A. Bonito, A. Demlow, and R. H. Nochetto. Finite element methods for the laplace–beltrami operator. In *Geometric Partial Differential Equations - Part I*, volume 21 of *Handbook of Numerical Analysis*, pages 1 – 103. Elsevier, 2020.
- [10] A. Bonito, A. Demlow, and J. Owen. A priori error estimates for finite element approximations to eigenvalues and eigenfunctions of the Laplace–Beltrami operator. *SIAM J. Numer. Anal.*, 56(5):2963–2988, 2018.
- [11] K. Deckelnick, G. Dziuk, and C. M. Elliott. Computation of geometric partial differential equations and mean curvature flow. *Acta Numer.*, 14:139–232, 2005.

- [12] A. Dedner and P. Madhavan. Adaptive discontinuous Galerkin methods on surfaces. *Numer. Math.*, 132(2):369–398, 2016.
- [13] A. Dedner, P. Madhavan, and B. Stinner. Analysis of the discontinuous Galerkin method for elliptic problems on surfaces. *IMA J. Numer. Anal.*, 33(3):952–973, 2013.
- [14] A. Demlow. Higher-order finite element methods and pointwise error estimates for elliptic problems on surfaces. *SIAM J. Numer. Anal.*, 47(2):805–827, 2009.
- [15] D. A. Di Pietro and A. Ern. *Mathematical aspects of discontinuous Galerkin methods*, volume 69 of *Mathématiques & Applications (Berlin) [Mathematics & Applications]*. Springer, Heidelberg, 2012.
- [16] G. Dong and H. Guo. Parametric polynomial preserving recovery on manifolds. *SIAM J. Sci. Comput.*, 42(3):A1885–A1912, 2020.
- [17] G. Dong and H. Guo. Superconvergence of differential structure on manifolds and its applications. *arXiv preprint*, pages 1–18, 2020.
- [18] Q. Du and L. Ju. Finite volume methods on spheres and spherical centroidal Voronoi meshes. *SIAM J. Numer. Anal.*, 43(4):1673–1692 (electronic), 2005.
- [19] G. Dziuk. Finite elements for the Beltrami operator on arbitrary surfaces. In *Partial differential equations and calculus of variations*, volume 1357 of *Lecture Notes in Math.*, pages 142–155. Springer, Berlin, 1988.
- [20] G. Dziuk and C. M. Elliott. Finite elements on evolving surfaces. *IMA J. Numer. Anal.*, 27:262–292, 2007.
- [21] G. Dziuk and C. M. Elliott. Finite element methods for surface PDEs. *Acta Numer.*, 22:289–396, 2013.
- [22] H. Guo. Surface Crouzeix-Raviart element for the Laplace-Beltrami equation. *Numer. Math.*, 144(3):527–551, 2020.
- [23] Jan S. Hesthaven and Tim Warburton. *Nodal discontinuous Galerkin methods*, volume 54 of *Texts in Applied Mathematics*. Springer, New York, 2008. Algorithms, analysis, and applications.
- [24] M. Kazhdan, M. Bolitho, and H. Hoppe. Poisson Surface Reconstruction. In Alla Sheffer and Konrad Polthier, editors, *Symposium on Geometry Processing*. The Eurographics Association, 2006.
- [25] Z. Li and Z. Shi. A convergent point integral method for isotropic elliptic equations on a point cloud. *Multiscale Modeling and Simulation*, 14(2):874–905, 2016.
- [26] J. Liang and H. Zhao. Solving partial differential equations on point clouds. *SIAM J. Sci. Comput.*, 35(3):A1461–A1486, 2013.
- [27] M. A. Olshanskii, A. Reusken, and J. Grande. A finite element method for elliptic equations on surfaces. *SIAM J. Numer. Anal.*, 47(5):3339–3358, 2009.
- [28] Béatrice Rivière. *Discontinuous Galerkin methods for solving elliptic and parabolic equations*, volume 35 of *Frontiers in Applied Mathematics*. Society for Industrial and Applied Mathematics (SIAM), Philadelphia, PA, 2008. Theory and implementation.
- [29] H. Wendland. *Scattered Data Approximation*, volume 17 of *Cambridge Monographs on Applied and Computational Mathematics*. Cambridge University Press, first edition, 2005.